Magyarhoni Földtani Társulat
Földtani Közlöny
Hungarian Geological Society

154/3, 277–298., Budapest, 2024

DOI: 10.23928/foldt.kozl.2024.154.3.277

A preliminary study on fluid migration pathways along the Rechnitz detachment fault – a tribute to Prof. Csaba SZABÓ

SPRÁNITZ, Tamás[1,2]*, TARI, Gábor[3], PORKOLÁB, Kristóf[1], VRŠIČ, Ales[4], HUJER, Wolfgang[4], MEKONNEN, Elias[4], BERKESI, Márta[1]

[1]MTA-EPSS FluidsByDepth Research Group, HUN-REN Institute of Earth Physics and Space Science, Budapest, Hungary
[2]Lithosphere Fluid Research Lab, Department of Petrology and Geochemistry, Institute of Geography and Earth Sciences, Eötvös Loránd University, Budapest, Hungary
[3]OMV Upstream, Vienna, Austria
[4]OMV Upstream, TECH Center & Laboratory, Gänserndorf, Austria
*spranitz.tamas@epss.hun-ren.hu

Előzetes eredmények a Rohonci-nyírózóna fluidumáramlási útvonalairól – tisztelgés SZABÓ Csaba professzor munkássága előtt

Összefoglalás

A Szombathely-II. (rövidítve: Szh-II) magfúrás a magyarországi Duna-medence nyugati peremén teljes szelvénnyel 2150 m mélységben mélyült. A fúrás a megközelítőleg 2 kilométer vastagságú, neogén poszt- és szinrift medencekitöltő kőzetek alatt nemcsak a nagyon kisfokú-kisfokú metamorf paleozoós pre-rift Felső-Ausztroalpi (UAA) aljzatot érte el, hanem az alsó kréta Pennini-egység zöldpala fáciesű kőzeteit is. Az alpi aljzat egységeit egy nagy kiterjedésű laposszögű normálvető, a Rechnitz (Rohonci) vető/nyírózóna (detachment fault) választja el egymástól. Ez a vető felelős az osztrák–magyar határon húzódó Rechnitz-Eisenberg metamorf magkomplexum (Rohonci-ablak) kialakulásáért. Mivel a nagy kiterjedésű, extenziós nyírózónának a térségben nincsenek felszíni feltárásai, vizsgálatunk fókuszában a nyírózónát harántoló magfúrás kőzetanyaga áll, amelynek mikrotektonikai, diagenetikus, fluidum típus szerinti és repedezett rezervoár tulajdonságait mutatjuk be jelen tanulmányban. A Szh-II-es magfúrás anyagának különböző kőzeteiben elvégzett előzetes vizsgálataink a Rohonci-nyírózóna működéséről és a kapcsolódó potenciális paleofluidum áramlási útvonalairól szolgáltatnak új eredményeket.

A fő töréses deformációs zóna alatti Pennini zöldpala jól fejlett foliációt mutat, amelyet főként az aktinolit és a klorit irányítottsága definiál. A mintákban a milonitos mikroszerkezeti jelleg nem figyelhető meg, eszerint képlékeny nyírás nem volt jelentős a töréses nyírózóna alatt mintázott kőzetekben. A rideg deformáció mind a Pennini zöldpalát, mind a felette lévő UAA kőzetegységeket érintette. A devon karbonátok és kristályos palák egy vékony (mindössze 20 méter vastagságú) extenziós allochtont képviselhetnek a Rohonci-vető tetején, a neogén medencekitöltés alsó egységét jelentő konglomerátum alatt. Fluidumzárvány-vizsgálataink fókuszában a vető alatti Pennini zöldpala minták álltak, melyekben különböző bezáró ásványokban négy eltérő kemizmusú és eredetű fluidumzárvány típust különítettünk el. Apatitban elsődleges, részlegesen újranyílt CO_2±CH_4+H_2O összetételű fluidumzárványok örződtek meg (II.a, b, c típus). Az apatit és klinozoisit is befogadó ásványa továbbá másodlagos, azaz beforrt repedések mentén megjelenő kétfázisú (folyadék és gáz), rendre CO_2 és CH_4-tartalmú vizes fluidumzárványoknak (I. és II.d típus). A kőzet foliációját harántoló repedéskitöltő kalcitban primer fluidumzárványok (III. típus) őrződtek meg, amelyekben a folyadékfázisú H_2O mellett CO_2 és telített szénhidrogének mutathatók ki. Ezek bezáródása a kalciterek kristályosodásával lehetett egyidejű. Az erekben megjelenő kvarc alszemcsehatárai mentén kétfázisú CO_2-CH_4-N_2-tartalmú, vízgazdag fluidumzárványok (IV. típus) záródtak be, melyek a mikroszerkezeti megfigyelések alapján a képlékeny deformációval egyidejűleg a kvarc átkristályosodása során csapdázódtak. Fluidumzárvány petrográfiai vizsgálatok alapján a II.d és III. típusú fluidumzárványok esetén egyazon zárványcsoporton belül nagymértékben eltérő folyadék- és gázfázisra vonatkoztatott fázisarányok figyelhetők meg, ami a csapdázódáskor jelen lévő, vízgazdag fluidumrendszer felforrására (folyadék- és gázgazdag fázisok szeparációjára), így a fázisok heterogén csapdázódására utal.

A vizsgált vetőzóna felépítésének és működésének megismerése fontos felszín alatti geoenergetikai példát szolgáltathat a geofluidumok (víz és könnyűolaj) és különböző természetes gázok (CO_2, CH_4, N_2 és H_2) körülbelül 2 km mélységben történő migrációs útvonalainak feltárásához.

Tárgyszavak: Rohonci-nyírózóna, elsődleges fluidumzárvány, másodlagos fluidumzárvány, fluidummigráció, Pennini zöldpala, fúrómagléptékű szerkezeti vizsgálat

Abstract

The fully cored, 2150-m-deep Szombathely-II (abbreviated as Szh-II) well was drilled at the western margin of the Hungarian Danube Basin. Beneath a circa 2-km-thick Neogene post-to syn-rift basin fill, the well not only reached the pre-rift Upper Austroalpine (UAA) basement with its slightly metamorphosed Paleozoic units but also the underlying greenschists of the Lower Cretaceous Penninic unit. The Alpine basement units are separated by a large low-angle normal fault, which is the regional-scale Rechnitz (Rohonc) detachment fault. This fault was responsible for the formation of the Rechnitz–Eisenberg metamorphic core complex (MCC) straddling the Austrian–Hungarian border. Since the large-strain extensional Rechnitz detachment fault has no outcrops in the entire region, the core material was studied to characterize the fault penetrated in the borehole from a microtectonic, diagenetic, fluid migration and fractured reservoir point of view. This study presents the preliminary results on core samples with various lithology from the Szh-II well to better understand the Rechnitz detachment system and the corresponding fluid migration pathways.

The Penninic greenschist below the main brittle deformation zone exhibits a well-developed foliation defined mainly by the oriented growth of actinolite and chlorite; however, the lack of a high-strain mylonitic foliation suggests that ductile shearing was not fully localized beneath the brittle detachment fault at the well location. The subsequent dominantly brittle deformation affected both the Penninic greenschists and the overlying UAA units. The Devonian carbonates and schists may represent a thin (only 20-m-thick) extensional allochthon on the top of the Rechnitz detachment fault, but beneath the basal conglomerates of the Neogene basin fill.

Fluid inclusion studies targeted the Penninic greenschists in three samples beneath the detachment fault. Four types of fluid inclusions with variable chemistry and origin were distinguished in several host minerals. Apatite hosts primary CO_2±CH_4+H_2O fluid inclusions (Type IIa, b, c) indicating significant partial fluid loss. Secondary fluid inclusions along healed fractures were entrapped in apatite (Type IId) and clinozoisite (Type I) with a chemistry of CO_2+H_2O and CH_4+H_2O fluid, respectively. Vein-filling calcite, crosscutting the foliation of the rock, contains primary aqueous fluid inclusions (Type III) also containing CO_2 and indication of saturated hydrocarbons in the vapor phase, which were trapped along growth zones of the host mineral. Aqueous CO_2-CH_4-N_2-bearing two-phase fluid inclusions, referred to as Type IV inclusions, were found along subgrain boundaries of quartz veins. Textural analyses showing significantly different phase ratios within the same cluster of Type IId and Type III inclusions indicate that aqueous fluids were in or near to conditions of boiling during entrapment. Microstructural observations also indicate that carbonic fluid inclusions along grain-subgrain boundaries of quartz (Type IV inclusions) likely formed during ductile deformation and quartz recrystallization. Improved understanding of the architecture of this fault zone may provide insights into the energetics of subsurface migration of geo-fluids (water and light oil) and various natural gases (CO_2, CH_4, N_2 and H_2) at circa 2 km depth.

Keywords: Rechnitz detachment fault, primary fluid inclusions, secondary fluid inclusions, fluid migration, Penninic greenschist, core-scale structural analyses

Introduction

A proper understanding of fault zones has become increasingly important in geoenergy applications such as in hydrocarbon exploration and production, hydrogeological prospecting, geothermal exploitation, tectonic degassing, nuclear waste isolation, CO_2 sequestration and natural gas, as well ashydrogen storage design projects (AUBERT et al. 2021). Fault zones are commonly looked at in the context of being barriers to fluid and gas flow providing seals for various subsurface reservoir units (BERNAL 2024). However, fault zones can act as drains as well, compromising the reservoir to various degrees, the effect ranging from partial leakage to complete breach. Recent studies have demonstrated that fault zones may be both barriers and drains in space (HAINES et al. 2016) and time (PEI et al. 2015, AUBERT et al. 2022). The sequential development of broader fault zones may result early on in a fault network configuration with interconnected gas or fluid migration pathways, resulting in higher gas flux rates. However, mature fault zones may develop a very low permeability core due to cementation, and therefore the bounding damage zones become the effective pathways for migrating geofluids (ANNUNZIATELLIS et al. 2008).

A large low-angle normal fault, the regional-scale Rechnitz (in Hungarian: Rohonc) detachment fault is situated on the western flank of the Hungarian Danube Basin (*Fig. 1a*). Numerous exploration wells, drilled on both sides of the border, were integrated with reflection seismic data to differentiate between the lower versus upper plates of the major low-angle detachment faults, including the largest one responsible for the formation of the Rechnitz MCC (TARI et al. 2020). The regionally mapped Rechnitz detachment fault has a very large subsurface extent, on the order of 1000 km^2 (*Fig. 1a*). The first subsurface penetration of this major tectonic contact was reported by PAHR (1977) in the Maltern-1 antimony ore exploration borehole drilled to the west of the Bernstein Penninic Window in Burgenland (*Fig. 1a*). In this borehole a ~5-m-thick mylonite sequence was documented right beneath the detachment fault (PAHR 1977). Mylonites tend to be associated with high-strain extensional detachment faults in their footwall, especially in the case of MCCs (REYNOLDS & Lister 1990, AXEN 2019).

The study area within the Pannonian Basin is well-known not only for its small hydrocarbon finds and numerous seeps (KOVÁCS et al. 2018), noble gases, but also for the largest natural CO_2 field in Europe (PALCSU et al. 2014). Moreover, there is recent interest in potential natural hydro-

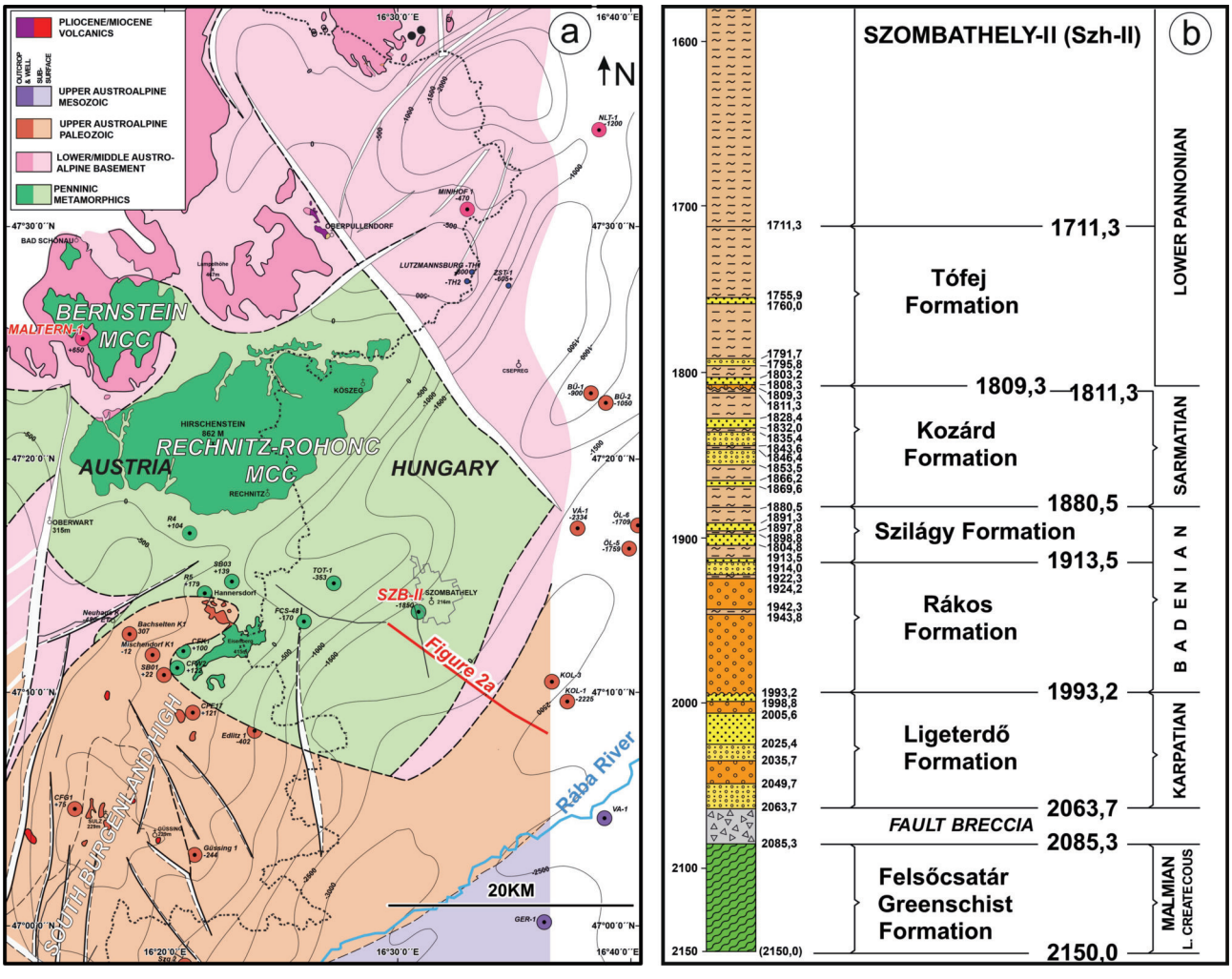

Figure 1. a) Subsurface geology of the broader Rechnitz area in the Alpine–Pannonian junction, modified from Kröll et al. (1988) and Tari et al. (2020). b) Lithostratigraphy of the Szh-II well in western Hungary based on detailed drill core sedimentological descriptions (Phillips et al. 1992). For a more detailed petrographic documentation of the deeper part of this well, see *Fig. 2.*

1. ábra. *a) A Rohonci-ablak és tágabb környezetének földtani egységei és elhelyezkedése az Alp-Kárpáti régióban (Kröll et al. 1988 és Tari et al. 2020 után módosítva). A nyugat-magyarországi Szh-II fúrás litosztratigráfiája a fúrómagok szedimentológiai leírása alapján (Phillips et al. 1992). A magfúrás által mintázott legalsó kb. 100 méter részletes kőzettani leírása a* 2. ábrán

gen generation associated with Penninic serpentinites in the footwall of the Rechnitz fault (Tari 2023).

The peculiarity of the Szombathely-II (abbreviated as Szh-II) well is that the syn-rift Miocene is directly overlying the detachment fault as broken-up blocks of Paleozoic carbonates with 15–20 m thickness, and that it can be considered as part of the damage zone of the Rechnitz fault. We assume that the degassing of the various gases generated in the basin fill and the basement below should have at least partially occurred along large detachment fault planes known in the basin (Tari 1996a, b). Therefore, the fully cored Szh-II well which penetrated the Rechnitz detachment fault, offers an exceptional opportunity to capture the potential signal of gas and fluid migration along the fault zone since the early Miocene.

Fluid droplets, trapped in crystallizing/recrystallizing minerals, are termed as fluid inclusions that serve as an effective tool to trace the stages of fluid flow. Fluid inclusions encapsulate a very small volume from the fluid migrating in the rock, thus permitting their direct study. Considering this, here we have distinguished various generations of fluid inclusions all likely indicating different fluid migration events that affected the studied rocks. In this study, we distinguished multiple fluid generations that once migrated in the greenschist at different stages of the rock's evolution (magmatic, metamorphic and ones contemporaneous with deformation events).

Regional geologic setting

Upper crustal extension in the NW Pannonian Basin occurred in two stages during the Miocene (Tari 1996a). As the first manifestation of extensional collapse at the beginning of the Early Miocene (~21–17.5 Ma, Ottnangian and early Karpatian) the Rechnitz metamorphic core complex (MCC) was formed (Ratschbacher et al. 1990, Tari & Bally 1990) in the Rába River extensional corridor. While

the Rechnitz MCC preserves relics of former subduction and nappe stacking processes related to the Alpine orogeny, the dominant metamorphic fabrics found in the complex are related to greenschist and sub-greenschist facies shearing representing the extensional exhumation of the Penninic formations (LELKES-FELVÁRI 1982, 1994; KUBOVICS 1983; KOLLER 1985; CAO et al. 2013). This metamorphic core complex style, ENE–WSW trending extensional phase may have produced as much as a minimum of 80 km horizontal extension (TARI 1996b). The early Miocene timing of the MCC extension was well constrained by several thermochronological studies in the Rechnitz Mts. (DEMÉNY & DUNKL 1991, DUNKL 1992, DUNKL & DEMÉNY 1997, CAO et al. 2013). Shortly after, and partly overlapping with this period, the style of syn-rift extension changed to a wide-rift style one (17.5–13.8 Ma, late Karpatian and Badenian) producing a minimum of 40 km extension in a NW-SE direction across the East Alpine/Pannonian transition zone. The predominance of low-angle normal faults in the Neogene structure of the Danube Basin (TARI et al. 1992, HORVÁTH 1993) is largely due to the second stage of syn-rift extension. The continuing, but gradually diminishing continental extension during the Late Miocene and Pliocene (12.5–5.5 Ma, Sarmatian–Lower Pannonian) could not advance to the localization of extension into a narrow rift zone in the NW Pannonian Basin, except perhaps in the center of the Danube Basin (TARI et al. 1999). The ongoing Pliocene fault activity was documented in the nearby Torony area (*Fig. 1a*) where Pannonian lignite beds were offset with a set of transtensional normal faults (KOVÁCS et al. 2015). However, it is the metamorphic core complex (MCC) style, ENE-WSW trending very high-strain extension and the subsequent lower strain wide-rift extension that played the key role in the Neogene structural evolution of our study area.

The Szh-II well was drilled in 1987–1988. A brief summary of the pre- and syn-rift lithologies encountered in the drill core is based on PHILLIPS et al. (1992). The stratigraphically lowest unit cored consists of 65 m (2085–2150 m) of greenschist (*Fig. 1b*), which represents the Lower Cretaceous Penninic unit of the Alpine nappe stack based on the lithologic analogy with the greenschists outcropping in the nearby Eisenberg and Rechnitz areas (*Figure 1a*), some 15 and 20 km to the W and NW (PAHR 1980, SCHMID et al. 1984, respectively). The schistosity (foliation) within this sequence is well-developed and shows a consistent dip between 45° to 50° throughout the cored interval.

Overlying the greenschists a 161-m-thick nonmarine sequence was drilled (1924–2085 m) with interbedded breccia, conglomerate, pebbly sandstone, and sandstone ranging in age from early to middle Miocene (Karpatian to Badenian). The basal strata resting on the greenschist consists of 21.4 m (2063–2085 m depth) of early Miocene (Karpatian) breccia (*Fig. 1b*). Angular clasts of schist, quartz, and dolomite as large as 5 cm set within a clast- or matrix-supported texture of pebbly sandstone or sandstone form the breccia. Schist forms the most abundant clast type. The breccia usually exhibits a chaotic fabric; however, poorly graded to well-graded beds as thick as 10 cm occur between unsorted intervals. We interpret these coarse clastic breccias as part of the brittle fault damage zone with meter-scale extensional allochthons in it, which explains the lack of a clear sedimentological classification of it (PHILLIPS et al. 1992).

Above the breccia unit is 139 m of early to middle Miocene (Karpatian to Badenian) sandstone and conglomerate forming an upward-coarsening sequence (*Fig. 1b*). The early Miocene (Karpatian) interval is 70 m thick (1993–2063 m depth). The strata consist of interbedded sandstone, pebbly sandstone, and conglomerate. A distinct 3-m-thick sandstone bed represents the stratigraphically youngest early Miocene (Karpatian) deposit. Most of the beds within this sequence are thin, ranging up to 40 cm in thickness. The conglomerate and sandstone beds may be graded and in places exhibit large-scale crossbedding. Lignite beds and laminae as well as silt laminae occur within a few of the sandstone beds. The conglomerate clasts are well-rounded and exhibit a clast- to matrix-supported texture. Some beds also have an unsorted fabric. We interpret this sequence as alluvial fanglomerates corresponding to the early MCC activity along the Rechnitz fault. The overlying fluvial to near coastal finer clastic sediments likely correspond to diminishing fault activity.

The middle Miocene (Badenian) conglomerate sequence (*Fig. 1b*) is 69 m (1924–1993 m) thick. The strata consist of massive to very-thick-bedded quartz and schist conglomerate characterized by a clast- to matrix-supported texture. The schist clasts range in size up to 30 cm and are well-rounded to subangular. Sandstone beds are greatly reduced in number in relation to the underlying early Miocene (Karpatian) strata. In places the clast-supported strata are poorly graded, but elsewhere they exhibit large scale cross-bedding or inverse grading. The fabric of many of the beds is disorganized. We interpret this sequence as a non-marine fault talus sequence corresponding to renewed brittle faulting during the Badenian rift-wide activity along several low-angle normal faults in the area (TARI et al. 1996a, b), one of them possibly superimposed on the earlier Rechnitz detachment fault (*Figure 2a*).

The work by LELKES-FELVÁRI (1994) aimed analyzing the lower 100 m of the core focusing on the Penninic metamorphic rocks and the Upper Austroalpine carbonate sequence. This greenchist sequence was described by LELKES-FELVÁRI (1994) as a green schistose rock, schistosity planes being parallel or folded, sometimes with sigmoidal folds. Layering or laminations highlighted by differences in mineral composition and grain size are widespread. The sequence is crosscut by carbonate veins. Chlorite, albite, epidote, actinolite were determined as the main mineralogical constituents of the Penninic sequence associated with titanite, minor quartz and white mica. The most widespread rock-types are greenschists and prasinites (albite+chlorite+epidote+titanite+actinolite). Chlorite-epidote schists and albite-rich rocks are present as thin layers. In some layers epidote-albite and actinolite-albite are abundant. They contain statically crystallized albites incorporating folded in-

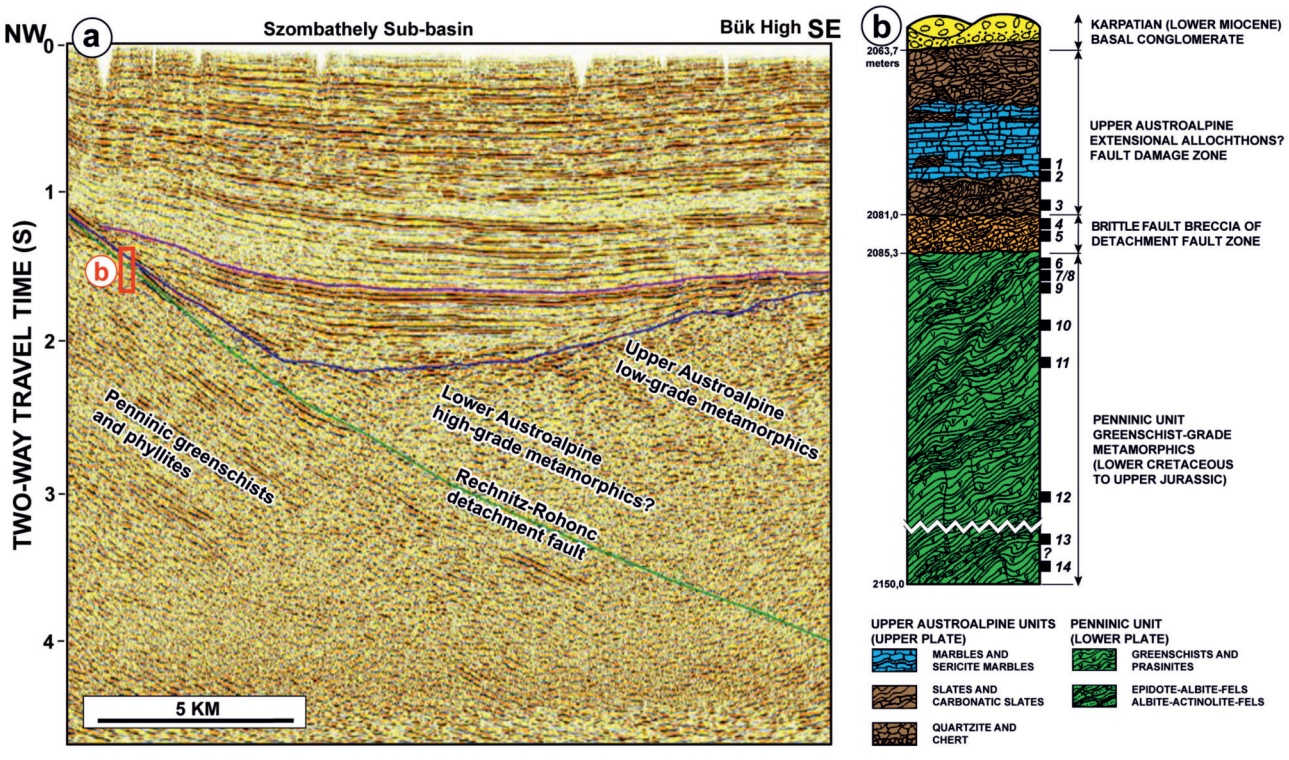

Figure 2. a) 2D reflection seismic data close to the Szh-II well (see *Fig. 1a*) illustrating the stratigraphic and structural context of the well (Tari et al. 1992). Red bracket indicates the location of b) Lithology of the pre-rift basement part of the borehole, adapted from Lelkes-Felvári (1994). The location of the 14 core samples (*Table I*) taken for various analytical work are also shown. Note that the lithology of Samples #4 and #5 in our analysis does not match the one shown by the litho-column

2. ábra. *a) A Szh-II fúrás környezetének rétegtani és szerkezeti sajátosságai 2D szeizmikus szelvény alapján (Tari et al. 1992). A* 2. ábra, b *helyét vörös téglalap jelöli. b) A fúrás által feltárt pre-rift aljzat litológiája Lelkes-Felvári (1994) munkája alapján, mely mutatja a jelen tanulmány tárgyát képező 14 minta helyzetét* (I. táblázat*). A 4-es és 5-ös számú minták pontos helyzete azonban nem egyezik meg a jelen rétegoszlopon ábrázolt pozíciókkal*

clusion trails. The relationship of crystallization to deformation of the minerals reveals a polyphase history for these rocks, which have a low-grade, greenschist metamorphic facies.

The overlying carbonate sequence was documented as containing interlayered slate and quartzite horizons. The whole sequence is strongly folded and brecciated, reflecting a wide variety of structures of composite ductile to brittle deformational style. The carbonate dominant unit contains fragments of marbles of different texture and composition. These marbles are lineated or granoblastic with subordinate, dispersed quartz, albite and/or preferentially oriented sericite crystals.

The interlayered slate and quartzite horizons and laminations are sericite slates, quartz-sericite-chlorite schist and sericite bearing quartzite. This sequence is crosscut by a singular, few-cm-thick mylonitic shear zone characterized by compositional layering and undulating trails of crushed material around porphyroclasts. The metamorphic grade of the carbonate-slate sequence was considered very low-grade by Lelkes-Felvári (1994).

Methods

The 14 core samples (5–10 cm long on average and 5 cm in diameter) were collected in the core repository of the Hungarian Geological Survey (currently: Supervisory Authority for Regulatory Affairs) in Pécs-Somogy. XRD and XRF analyses were performed on all 14 samples. Thin sections were prepared of twelve samples, and fluid inclusion analysis was performed on three samples. *Table I* lists the samples and corresponding analyses performed on each. XRD and XRF analyses, as well as petrographic description on thin sections were carried out in OMV Upstream, TECH Center & Laboratory in Gänserndorf, Austria. Thin sections were stained in order to better distinguish the sequence of vein formations in the studied samples. The main goal was to characterize the nature of the Rechnitz fault zone (diagenesis, reservoir properties) as potential migration channels for natural gases and fluids. A secondary objective was to petrographically describe the microtectonic features of the Penninic greenschists beneath the Rechnitz detachment fault.

X-ray diffraction (XRD) analysis

X-ray diffraction (XRD) analysis complemented by thin-section analyses was used to determine the bulk mineralogical composition (*Table II*). We used a Bruker AXS D8 Advance X-ray diffraction spectrometer (copper Kα radiation generated X-ray tube at 40 kV and 40 mA, and X-ray detector Lynxeye XE-T) and the software DIFRAC.EVA V3 to identify different mineral phases. Sample preparation included grinding to a fine powder in an agate mortar or a

Table I. Summary table of the studied samples showing the corresponding depth, lithology and applied methods described in the manuscript. Please note that 'Fluid inclusions' comprises fluid inclusion petrography and Raman spectroscopy (on the inclusions)

I. *táblázat.* *Összefoglaló táblázat a vizsgált minták mélységéről, litológiájáról és a jelen munkában bemutatott vizsgálati módszerekről. A „Fluid inclusions" jelölés fluidumzárvány petrográfiai és Raman-spektroszkópos vizsgálatok együttes elvégzését jelöli*

#Sample	Depth (m)	Lithology	XRD, XRF	Thin section	Fluid inclusion
1	2075.7	Slate/Phyllite	X	X	
2	2076.9	Slate/Phyllite	X	X	
3	2080.4	Limestone	X	X	
4	2082.4	Greenschist	X	X	
5	2083.1	Greenschist		X	
6	2086.9	Greenschist	X	X	
7	2087.1	Greenschist		X	
8	2087.7	Greenschist	X	X	
9	2088.2	Greenschist	X	X	
10	2091.9	Greenschist	X	X	
11	2094.2	Greenschist	X	X	X
12	2114.8	Greenschist	X	X	
13	2135?	Greenschist	X	X	X
14	2145?	Greenschist	X	X	X

swing mill; samples were then placed in a plastic sample holder, keeping a flat upper surface to achieve a random distribution of lattice orientations. For quantification of the minerals detected by XRD, the software TOPAS (Total Pattern Analysis Software) was used. The TOPAS software utilizes the Rietveld method based on analytical profile functions and least-squares algorithms to achieve the best fit between a theoretical and a measured pattern.

X-ray fluorescent (XRF) spectroscopy

XRF analyses provided the bulk chemical composition of the studied samples (*Table III*). The elemental analysis was performed using a Panalytical EPSILON 3 XL Energy-dispersive X-ray fluorescence spectrometer (Ag radiation with software-controlled max. 50 kV, max. 3 mA and 15 W tube power equipped with a silicon drift detector). The Epsilon 3 software was used for qualitative and semi-quantitative analyses, and this included the Omnian software module for standardless and fingerprint applications. The detection limit was assumed to be less than 1.0 wt.% or less for individual elements.

Core-scale structural observations

Macroscopic structural and lithological features were characterized for the entire cored section of the Szh-II well, with special focus on the 14 core samples. In particular, we identified macroscopic mineral assemblages, vein generations, as well as brittle (fractures and faults) and ductile (tectonic foliation, stretching lineation, folds, shear bands) deformation features. These macroscopic observations were

Table II. Bulk mineralogical compositions of the 14 samples from the Szh-II well based on XRD measurements. Values are expressed in weight percent

II. táblázat. *Az Szh-II fúrásból származó 14 minta modális összetétele, XRD-vizsgálatok alapján. Az értékek tömeg%-ban vannak kifejezve*

#Sample	Depth (m)	Albite	Dolomite	Ankerite	Calcite	Quartz	Siderite	Pyrite	Sericite	Clinochlore	Clinozoisite	Actinolite	Titanite	Anatase	Fluor apatite
1	2075.7	51.52		11.16	0.02	9.79	12.26		4.51	5.16				3.49	2.09
2	2076.9	16.59	17.91	12.22	18.93	11.64	3.8		11.32	4.69				2.9	
3	2080.4		3.85	5.21	83.55	7.39									
4	2082.4	9.47		2.32	10.37	15.7				59.41		2.73			
5	2083.1	16.77	0.54		13.71	18.28		0.05		50.65					
6	2086.9	30.3			7.18	2.15				48.79		8.15	3.43		
7	2087.1									54.4		45.6			
8	2087.7					1.35				21.98		76.67			
9	2088.2	17.66			8.3	7.18				48.75	9.95	3.81	4.35		
10	2091.9	30.26			7.7	4.03				31.54	9.49	13.89	3.09		
11	2094.2	19.82								19.27	21.44	36.21	3.26		
12	2114.8	35.38			5.55	5.28				19.22	19.79	12.47	2.31		
13	2135?	31.37								20.07	14.08	30.42	4.06		
14	2145?	18.35				1.88				30.33	15.61	30.56	3.27		

Table III. Bulk major and trace element composition of 14 samples from Szh-II well, based on XRF analysis. Values are expressed in weight percent
III. táblázat. *A Szh-II fúrásból származó 14 minta teljes kőzetösszetétele, XRF-vizsgálatok alapján. Az értékek tömeg%-ban vannak kifejezve*

#Sample	Depth (m)	SiO_2	TiO_2	Al_2O_3	Cr	Fe_2O_3	MnO	Ni	MgO	CaO	Na_2O	K_2O	P_2O_5	SO_3	Cl	V	Sr	Ba
1	2075.7	45.89	3.79	21.32	0.01	12.84	0.19		2.82	7.22	4.81	0.10	0.75	0.02	0.20	0.02		
2	2076.9	34.79	2.98	16.75	0.04	11.36	0.24		4.34	26.24	1.55	1.34		0.06	0.20	0.04	0.04	0.03
3	2080.4	9.15	0.04	0.53	0.01	1.55	0.06		2.47	85.58		0.26		0.24	0.05		0.06	
4	2082.4	40.72	0.64	16.10	0.36	10.95	0.15	0.09	2.,79	8.66		0.35		0.06	0.12	0.02		
5	2083.1	43.06	0.84	15.38		10.72	0.16	0.08	19.37	9.91		0.27		0.06	0.12		0.03	
6	2086.9	40.76	0.9	19.53	0.05	10.93	0.16	0.03	18.62	6.52	2.34	0.04			0.11	0.02		
7	2087.1	42.26	0.31	13.18	0.15	10.96	0.20	0.11	24.96	7.69		0.06			0.11	0.01		
8	2087.7	51.51		5.25	0.09	7.43	0.17	0.12	22.31	12.95		0.07			0.09	0.01		
9	2088.2	39.00	1.27	19.26	0.05	12.46	0.17		16.62	9.38	1.58	0.03		0.06	0.09	0.03		
10	2091.9	44.65	1.03	17.66	0.04	10.18	0.15		12.01	10.64	3.44	0.06		0.03	0.10	0.02		
11	2094.2	45.41	0.89	16.48	0.04	10.10	0.16		13.24	11.69	1.80	0.06		0.02	0.09	0.02		
12	2114.8	47.31	0.81	18.75	0.04	7.90	0.13		9.56	11.26	3.98	0.10			0.10	0.02	0.02	
13	2135?	48.62	0.79	16.28	0.05	8.95	0.22		11.28	9.58	3.85	0.10		0.17	0.10	0.02		
14	2145?	45.07	0.92	16.62	0.05	11.79	0.17		14.14	9.03	1.96	0.08		0.07	0.09	0.02		

used to select core samples and to delineate prospective areas for microscale analyses.

Fluid inclusion methodology

Doubly-polished 100-µm-thick sections were prepared to describe and analyze fluid inclusion generations from three selected greenschist samples. Fluid inclusion petrography was conducted using a Nikon OptiPhot2 optical microscope equipped with a Nikon CoolPix DS-Fi1 camera system in the Lithosphere Fluid Research Laboratory, Eötvös Loránd University (ELTE), Hungary. Raman spectroscopy was performed using a Horiba JobinYvon Labram HR800 spectrometer with Nd-YAG (λ = 532 nm) and also He-Ne (λ = 633 nm) laser excitation in the Research and Industrial Relations Center (ELTE). The analytical settings included 100× objective, 50–100 µm confocal hole, 10–200 s acquisition time, 2× accumulations within the spectral range of 100–4250 cm^{-1}. Raw spectra were evaluated using LabSpec v.6 software. Raman bands of analyzed phases were identified based on the RRUFF database (Lafuente et al. 2015, Frezzotti et al. 2012). Molar ratios of fluid phases within inclusions, such as CO_2 and CH_4 were determined based on integrated band areas (Dubessy et al. 1989). The aim of Raman spectroscopic measurements was to define the chemistry of different phases within fluid inclusions.

Petrography

Phyllite

Samples #1–2 represent the UAA in the hanging wall (which might be the damage zone part) of the Rechnitz fault, between ~ 2063–2085 m (*Fig. 1*). These rocks are made up mostly of albite, quartz, white mica (sericite) and chlorite. Rock foliation is defined by white mica, chlorite and leucoxene (fine-grained alteration products of titanium-rich minerals) bands (*Figs 3a–b*). Veins filled by carbonate and quartz occur crosscutting the foliation of the rock. The following sequence of veins can be established according to textural observations: 1) ferroan calcite, 2) ferroan dolomite, 3) quartz. The foliation and some carbonate veins are postdated by brittle deformation represented by fragmentation of quartz/albite/sheet-silicate/carbonate-rich domains, whereas ferroan dolomite then quartz cementation took place after this deformation event (*Fig. 3c–d*). Albite and quartz occur as 5–50-µm-sized anhedral grains associated with an oriented network of fine-grained fibrous white mica and chlorite (*Fig. 3a–b*). The modal percentages of minerals in the phyllite are plagioclase (albite) 17–52%, quartz 10–12%, sericite 5–11%, chlorite (clinochlore) ~5%, leucoxene (anatase) ~3% and carbonates 23–53% (*Table II*).

Limestone cataclasite

The rock (Sample #3) mainly consists of limestone clasts embedded in a fine-grained cataclasite matrix (*Figure* 3e). Limestone clasts, with size ranging from 10 µm to 2-3 mm, are angular, cracked and made up by calcite. The matrix consists of saddle dolomite, poikilotopic ferroan calcite and quartz (*Fig. 3f*). Textural analyses suggest the following sequence of diagenetic events: after the brittle cataclastic deformation the microporous matrix was first dolomitized and later infiltrated by acidic pore waters, which favored calcite dissolution and silica cementation. The microporous matrix was preferentially dissolved while the clasts remained almost intact (*Fig. 3f*). There were also open fractures where quartz precipitated. The pore water chemistry changed for a second time when ferroan calcite precipitated (*Fig. 3f*).

Greenschist

Samples #4–12 represent greenschists in the footwall of the Rechnitz fault. We found that sample #4 at the depth of 2082.4 m is a greenschist contrary to the designation of this depth level as a fault breccia by LELKES-FELVÁRI (1994), see *Fig. 2b*.

The rocks consist predominantly of actinolite, chlorite, albite, clinozoisite, whereas titanite and apatite occur in minor quantities. The greenschist is locally made up almost exclusively by actinolite or chlorite (*Fig. 4a*). The modal percentages of minerals in the greenschists are actinolite 3–77%, chlorite (clinochlore) 19–59%, plagioclase (albite) 9–36%, clinozoisite 0–21%, carbonates 0–14%, quartz 0–18% and titanite 0–4% (*Table II*). Note that although XRD measurements did not indicate the presence of apatite in the greenschist samples, few grains were found in Sample #14 (see below in section *Fluid inclusions characteristics*). Actinolite forms 0.1–1-mm-sized euhedral fibrous-radial crystals (*Fig. 4a*), while chlorite is dominantly anhedral with grain

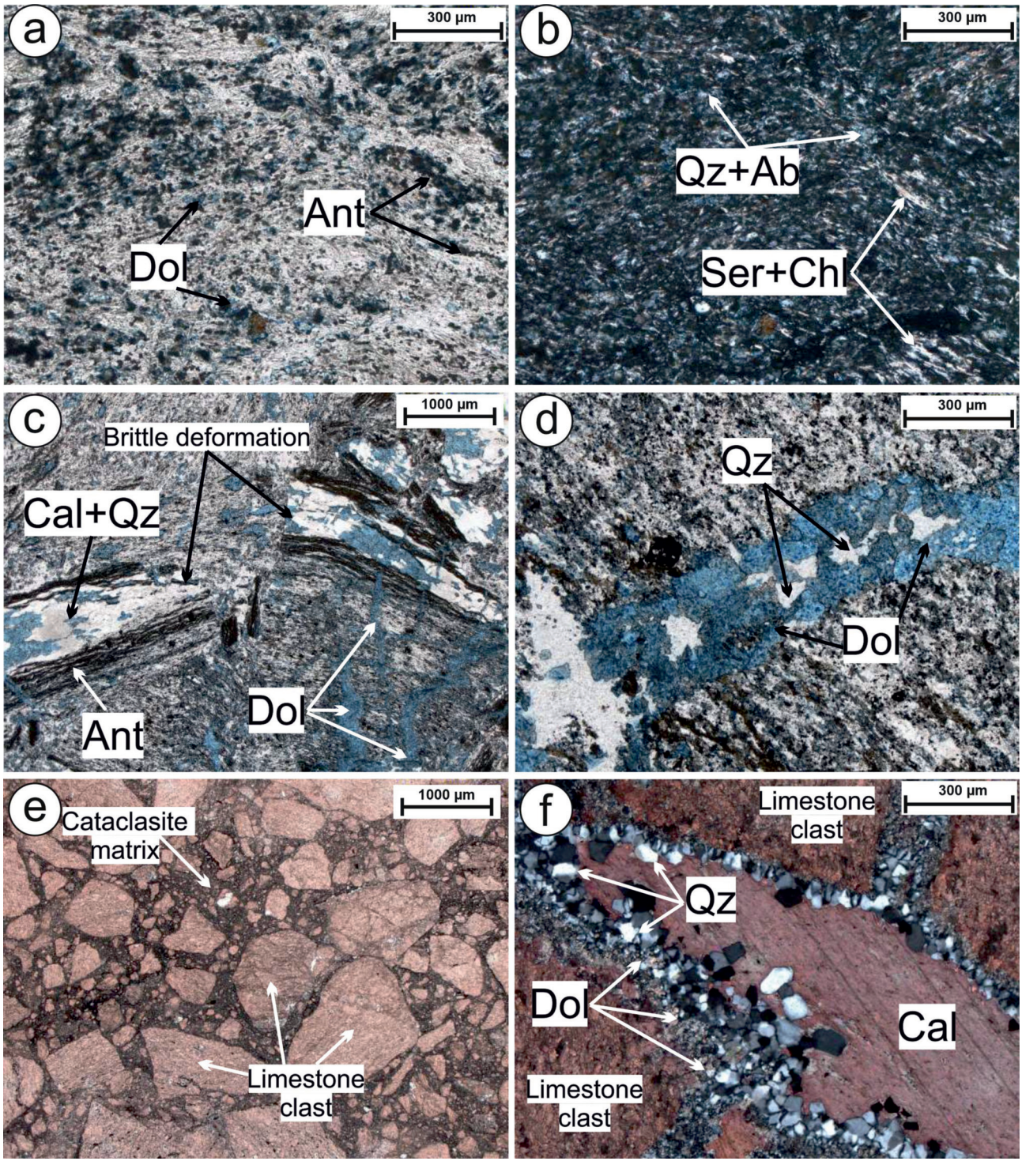

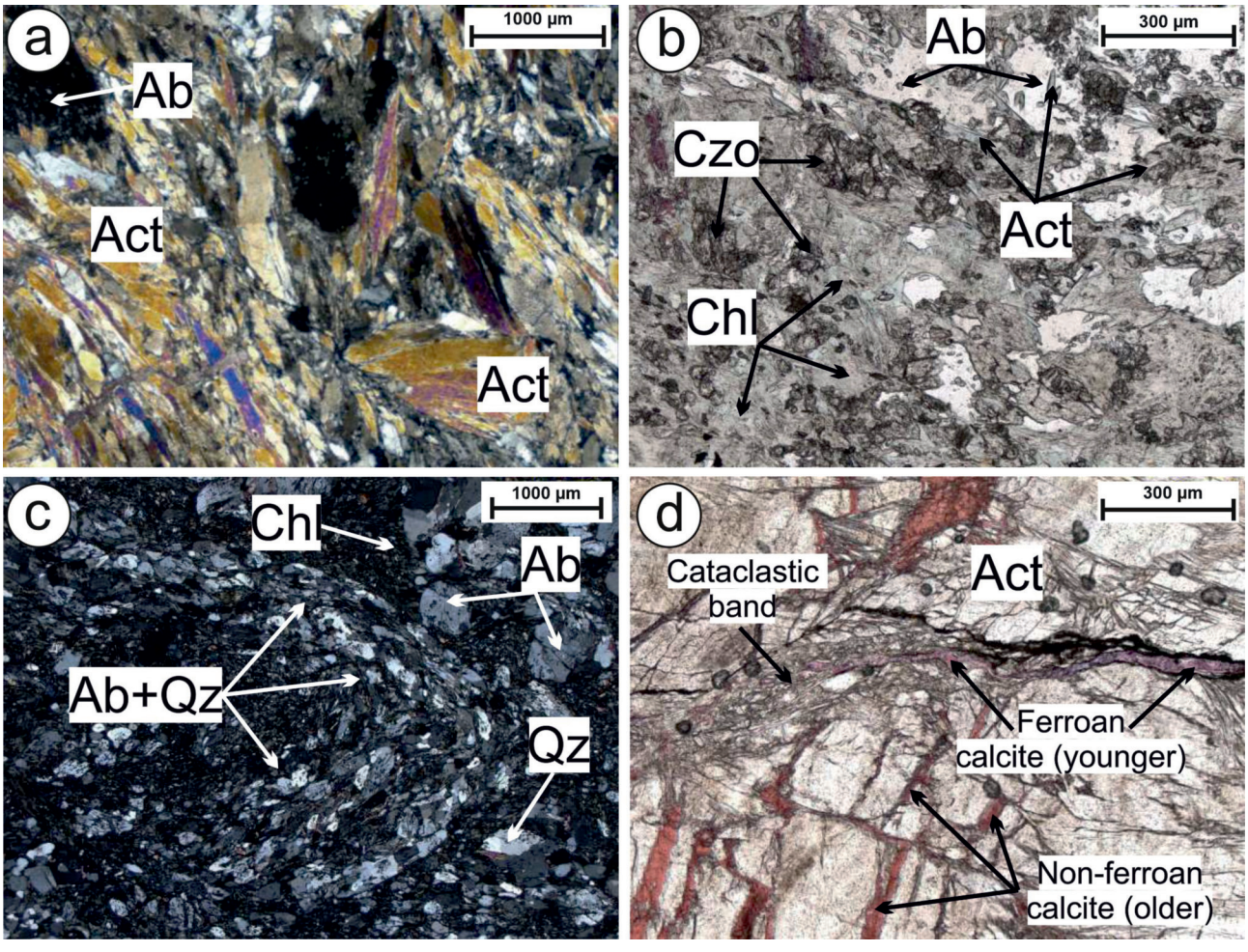

Figure 4. Photomicrographs presenting petrographic characteristics of greenschist samples (#4-12) from the Penninic unit in the footwall of the Rechnitz fault (a, c: cross polarized; b-d: plane polarized; a–d: transmitted light). a) Fibrous-radial actinolite occurring as the major rock-forming mineral in the greenschist samples. b) Albite and clinozoisite occur as slightly elongated grains embedded in the oriented network made up by actinolite and chlorite. c) Chlorite associated with albite and quartz commonly show signs of ductile deformation as forming shear bands and folds. d) Brittle deformation is represented by cataclastic bands, where actinolite and albite crystals are partly crushed and associated with younger calcite cemented fractures, which are postdating non-ferroan calcite veins

Abbreviations: Act – actinolite, Chl – chlorite, Qz – quartz, Ab – albite, Czo – clinozoisite

4. ábra. *A Rohonci-vetőzóna talpi blokkjához tartozó Pennini zöldpala minták (4-12-es számú) főbb petrográfiai sajátosságai (a, c: +N; b-d: 1N; a-d: áteső fény). a) Tűssugaras aktinolit, mely a minták legfőbb kőzetalkotó ásványaként jelenik meg. Az aktinolit és albit kristályok a rideg deformáció hatására töredezettek, repedezettek. b) Az aktinolit és klorit irányított hálózatában ahhoz illeszkedő orientációban enyhén megnyúlt albit- és klinozoisitszemcsék jelennek meg. c) Az albit- és kvarcszemcsékhez kapcsolódó klorit gyakran nyírási szalagokat formal, mely képlékeny deformáció hatására jött létre. d) A mintákban a rideg deformáció kataklasztosodott zónák, erek kialakulását okozta, melyhez vasban gazdag kalcit cementációs fázis kötődött. Előbbi eseményeket megelőzően vasban szegény kalciterek képződtek*

Rövidítések: Act – aktinolit, Chl – klorit, Qz – kvarc, Ab – albit, Czo – klinozoisit

← **Figure 3.** Photomicrographs showing characteristic petrographic features of samples from the Upper Austroalpine unit in the hanging wall (Sample #1-2: phyllite, Sample #3: catalastic limestone), which is considered as the damage zone of the Rechnitz fault (a, c, d, e: plane polarized, b, f: cross polarized, a-f: transmitted light). a-b) In phyllite albite and quartz grains are embedded in an oriented network of white mica (sericite), chlorite and leucoxene defining the foliation of the rock. c) Typical brittle deformation textures in phyllite showing fragmentation of the foliation and quartz/albite/sheet-silicate/carbonate-rich domains which is followed by ferroan dolomite cementation. d) Ferroan dolomite then quartz cementation in the studied phyllite occurred after brittle deformation as shown on image c. e) Characteristic texture of cataclastic limestone showing carbonate clasts with angular shape and wide range of grain size embedded in a fine-grained matrix. f) In cataclastic limestone, brittle deformation was followed by diagenetic events, represented by the following structures in chronological order: 1) saddle dolomite formation, 2) silica cementation producing quartz precipitation in fractures, 3) poikilotopic ferroan calcite cementation, for details see text

Abbreviations: Ant – anatase (leucoxene), Dol – dolomite, Qz – quartz, Ab – albite, Ser – sericite, Chl – chlorite, Cal – calcite

← ***3. ábra.*** *A Felső Ausztroalpi egység kőzeteinek főbb petrográfiai tulajdonságai (1-es és 2-es számú minta: fillit, 3-as számú minta: mészkő kataklázit), melyek a Rohonci-nyírózóna leginkább repedezett egységét reprezentálják. (a, c, d, e: 1N, b, f: +N, a-f: áteső fény). a-b) A fillit foliációját meghatározó fehér csillámból (szericit), kloritból és leukoxénből álló irányított hálózatban albit- és kvarcszemcsék találhatók. c) Rideg deformációs mikroszerkezetek fillitben: a kvarcban/albitban/rétegszilikátokban /karbonátban gazdag egységek feldarabolódása, melyet vasban gazdag dolomit cementációs fázis követett. d) A rideg deformációt vasban gazdag dolomit, majd kvarc cementációs fázis követték. e) A mészkő kataklázit jellegzetes mikroszövete, melyben a szögletes, nagyon változó méretű karbonátklasztokat finomszemcsés mátrix veszi körül. f) A mészkő kataklázitban a rideg deformációt az alábbi diagenetikus események követték, időrendi sorrendben: 1) nyeregdolomit képződése, 2) kovás cementációs fázis, melynek eredményeként a repedésekben kvarc kristályosodott, 3) poikilotópos vasban gazdag kalcit cementáció (részleteket ld. szöveg)*

Rövidítések: Ant – anatáz (leukoxén), Dol – dolomit, Qz – kvarc, Ab – albit, Ser – szericit, Chl – klorit, Cal – kalcit

size between 10–500 µm (*Fig. 4b*). Albite and clinozoisite occur as 50–400-µm-sized isometric, slightly elongated grains embedded in the oriented network made up by actinolite and chlorite (*Fig. 4b–c*).

Quartz and calcite/ferroan calcite occur as inter- and intracrystalline fracture fillings. Actinolite and chlorite, defining the foliation of the rock, commonly show signs of ductile deformation forming shear bands and folds (*Fig. 4c*), although mylonitic textures are absent. Our microstructural analysis showed the lack of dramatic grain size reduction, (i.e., mylonitization) in the greenschist. Microstructural analyses confirmed the macroscopic observations as to a general lack of mylonitic fabric within the greenschists. Still, we observed a well-developed foliation and moderate folding that demonstrate ductile deformation prior to brittle faulting. Brittle deformation is represented by cataclastic bands, where actinolite and albite crystals are partly crushed and associated with calcite cemented fractures (*Fig. 4d*). Textural analyses showed that, in some samples, a younger ferroan calcite cement generation is synchronous with cataclasis, evidenced by cross-cutting the non-ferroan calcite cement (*Fig. 4d*).

Implications based on bulk XRF data

XRF analysis was carried out on all samples to provide the weight percent of major to trace elements (*Table III*). As already proved by LELKES-FELVÁRI (1994), data from XRF analysis can be used to prove the Penninic origin of the greenschists as opposed to being equivalents to the Paleozoic greenschists occurring in the Graz Paleozoic or the ones outcropping at Hannersdorf (*Fig. 1*). Among the major elements, TiO_2 and P_2O_5, and the trace elements Ni, Cr and V can be used for this discrimination (see *Fig. 5*). The values reported by LELKES-FELVÁRI (1994) from the Szh-II well match the ones obtained in this study from 10 greenschists samples (*Table III*). Moreover, the major element variations in SiO_2 and CaO, for example, provide additional evidence for the lithologic discrimination of the UAA phyllites, limestones and the Penninic greenschists described above (*Table III*).

Core-scale structural observations

The syn-rift conglomerates and fanglomerates (PHILLIPS et al. 1992) are directly underlain by a significant zone of brittle deformation showing high fracture density and intense brecciation of various lithologies (*Fig. 2b*); these are regarded as a branch of the Rechnitz/Rohonc detachment system. The main part of this deformation zone, where fracture density is substantial on the hand specimen scale, is ca. 20 m thick and largely consists of cataclastic carbonates with slate and quartzite lenses (*Fig. 6a*). At the base of the deformation zone, the carbonate and slate material is mixed with the underlying greenschists, forming a purple to green fault breccia. The carbonate-dominated upper lithology was interpreted as Paleozoic UAA (correlated by the Graz Paleo-

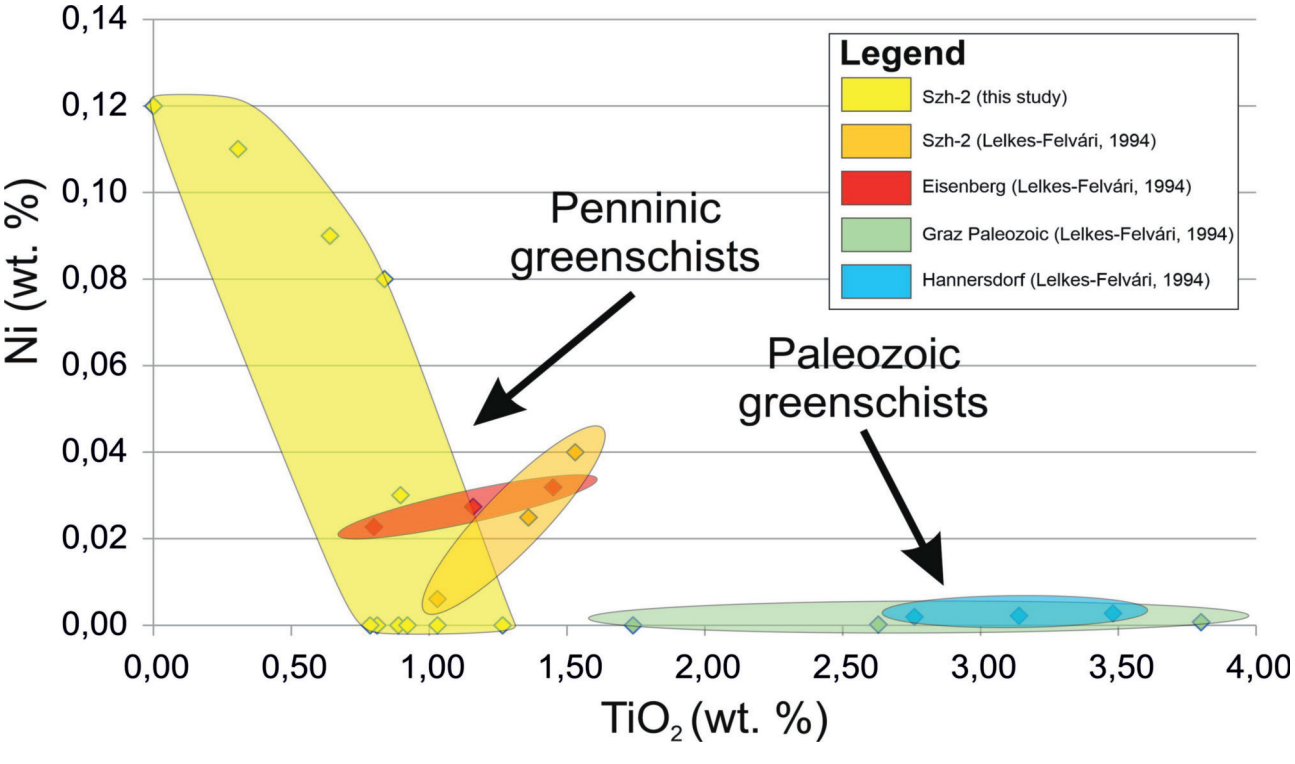

Figure 5. Chemical variation diagram showing TiO_2 vs. Ni content (in wt.%) in bulk greenschist samples based on XRF analyses. As comparison, bulk rock compositions described by LELKES-FELVÁRI (1994) for the same and similar rock types are also indicated. For details see text

5. ábra. *A vizsgált zöldpala minták teljes kőzet összetételének TiO_2 vs. Ni tartalma (tömeg%-ban kifejezve) XRF-mérések alapján. A diagramon feltüntetésre kerültek összehasonlításként LELKES-FELVÁRI (1994) által közölt, ugyanazon rétegsor egyes elemeire, további hasonló kőzetekre vonatkozó mérési eredményei is (részletek a szövegben)*

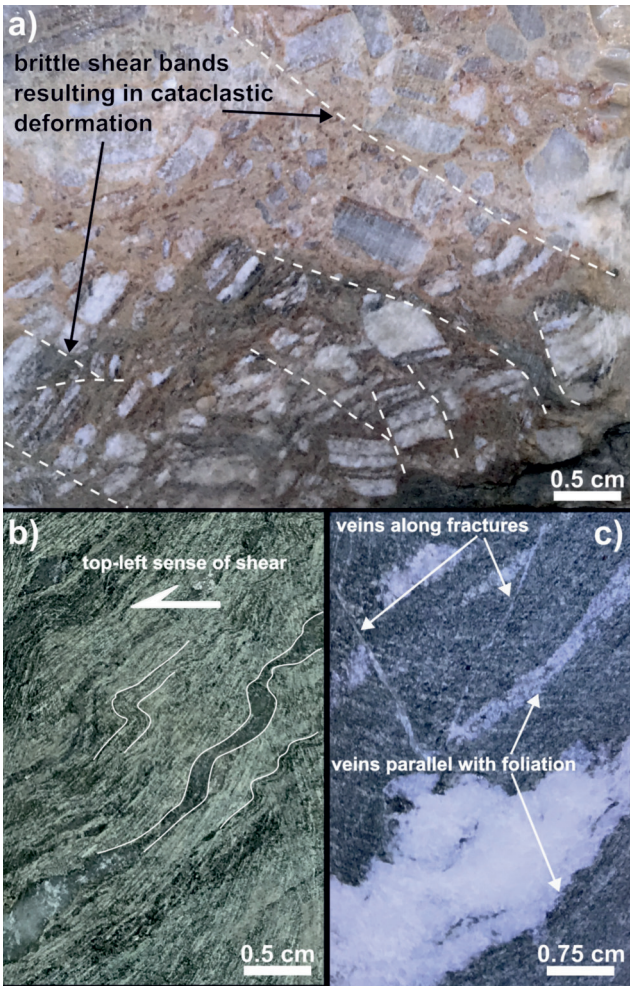

Figure 6. Core-scale structural characteristics of the studied samples. a) Fault breccia within the main deformation zone mostly containing carbonate clasts, exhibiting microfaults and cataclastic deformation (sample #2, flat surface). b) Penninic greenschist below the fault zone exhibiting a well-developed foliation and asymmetric folds, implying moderate shearing (sample #12, flat surface). c) Penninic greenschist below the fault zone exhibiting foliation-parallel and fracture-parallel calcite veins (photo of the mantle of the core). Large foliation-parallel veins imply the creation of significant transient porosity during or after metamorphism

6. ábra. *A vizsgált minták fúrómagléptékű szerkezeti sajátosságai. a) A fő deformációs zónában található vetőbreccsa (2-es számú minta), melyben a karbonát klasztok rideg deformáció okozta nyírási szalagok mentén rendeződtek és kataklasztosodtak. b) A nyírózóna alatt elhelyezkedő Pennini zöldpala jól fejlett foliációt mutat és aszimmetrikus redőket formal, melyek közepes nyírás hatására jöhettek létre. c) A nyírózóna alatt elhelyezkedő Pennini zöldpalában a foliáció síkjával és a repedésekkel párhuzamosan kalcit erek jelennek meg. A foliációval párhuzamos erek fejlődése jelentős átjárható porozitás kialakulására utal a metamorfózis során*

zoic by Lelkes-Felvári 1994), while the greenschists belong to the Penninic unit.

Observations show that the weakly to moderately foliated Paleozoic rocks of the UAA unit are broken into angular pieces ranging from sub-mm to several cm (*Fig. 6a*) over the entire thickness of the fault zone. This intense cataclastic deformation only affected the uppermost few meters of the Penninic greenschist. The greenschist shows a well-developed foliation (*Fig. 6b*) below the detachment fault, attesting to ductile fabric formation prior to the localization of the detachment. The foliation in the greenschist is mainly defined by the oriented growth of actinolite and chlorite (also defining stretching lineations on some foliation planes) and subordinately by albite and clinozoisite. The foliation has a dip angle between 20 and 40 degrees and is affected by minor to moderate folding. Besides the gentle folding that causes the slight variance of the foliation dip angle, an open to tight asymmetric fold population was also observed (*Fig. 6b*) that consistently indicates a downdip shearing direction (presumably in agreement with the kinematics of the subsequent brittle detachment fault). The greenschists are also affected by significant vein generation. Veins are made up of calcite and quartz and are mostly oriented parallel with the main foliation (*Fig. 6c*). Veins also grew along post-foliation fractures that are found both parallel with and also at a high angle with respect to the foliation (*Fig. 6c*). Veining in general shows that the Penninic greenschists have undergone alterations (mineral reactions, fracturing) that created significant transient porosity. This porosity was then used by fluids focused along the deformation zone and subsequent precipitation filled this porosity. The foliation of the greenschists does not show signs of significant mylonitization, such as well-developed shear fabrics or substantial grain size reduction.

Fluid inclusion characteristics

Three samples (Samples #11, 13 and 14, *Fig. 7*) from the Penninic greenschists in the footwall of the Rechnitz fault were selected for fluid inclusion analysis. Multiple types of fluid inclusions occur hosted by the different, mostly accessory minerals (oriented apatite and clinozoisite along with the foliation of the rock) and also in vein-filling minerals such as quartz and calcite. These veins are almost always parallel with the foliation of the rocks, although calcite veins occur with high angle compared to the direction of the foliation (*Fig. 7*). Calcite veins are up to 3 mm thick, whereas few-hundred-micron-thick veinlets also occur, the latter most commonly cross-cutting rock foliation. Fluid inclusions are hosted by thicker, 1–2-mm-thick veins with similar petrographic characteristics in both the foliation cross-cutting veins and in the foliation-parallel veins. Vein-forming calcite grains are 5–100-μm-sized and typically show straight grain boundaries with granoblastic texture (see *Fig. 9b*).

Quartz veins are 200–2000 μm thick and show folded structures parallel with the foliation of the rock. As an alternative interpretation, these structures may not be real veins. Rather, these might be quartz lenses, which were deformed during metamorphism and related to the metamorphic foliation. Quartz grains and subgrains are 10–100-μm-sized and contain fluid inclusions most commonly along sub-grain boundaries (*Fig. 9g*).

In the following, petrographic observations and results from Raman spectroscopy will be described together.

Type I inclusions are hosted by clinozoisite and form 1–15 μm elongated, strained and irregular shaped secondary

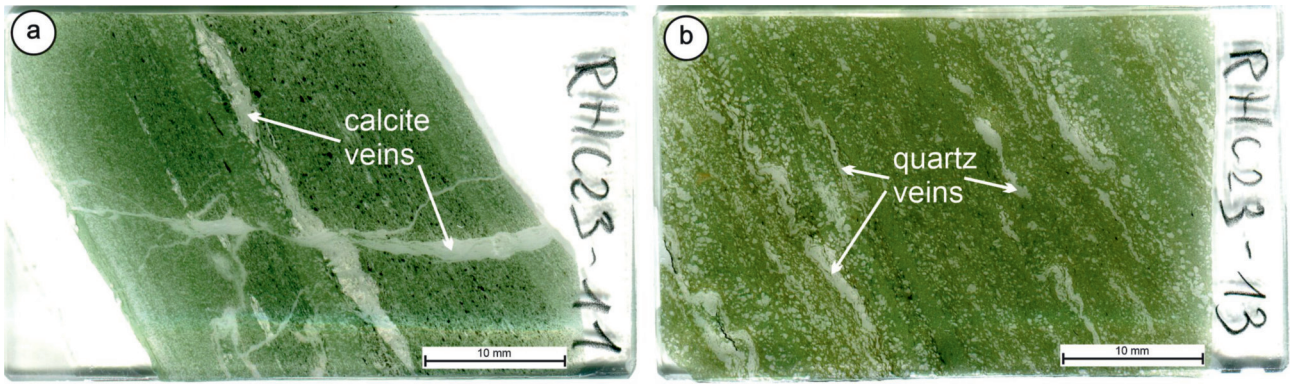

Figure 7. Scanned images of the thick sections prepared for fluid inclusion analyses of the studied greenschist samples (Sample 11 and 13) showing different vein textures. a) Calcite veins running parallel and at high angle with the rock foliation. b) Quartz veins parallel with the foliation

7. ábra. *A vizsgált (11. és 13. számú) zöldpalamintákból, fluidumzárvány-vizsgálatokhoz készített vastagcsiszolatok szkennelt képei, melyeken különböző értípusok figyelhetők meg. a) A kalciterek a foliációval párhuzamosan, illetve attól jelentősen eltérő szögben jelennek meg. b) Kvarcerek kizárólag a kőzet irányítottságával párhuzamosan húzódnak*

two-phase (liquid and vapor) fluid inclusions at room temperature (*Fig. 8a, b*). Raman spectroscopy shows CH_4 in the vapor phase and H_2O in the liquid phase (*Fig. 10*) together with accidentally trapped few-micron/submicron-sized solid phases, such as calcite. Phase ratios are generally constant in this type of fluid inclusions, which indicates homogeneous (one-phase) entrapment.

Oriented apatite is rich in fluid inclusions, representing multiple generations (Type II a–d).

Tubular, 2–3-μm-long, highly stretched and most likely opened primary two-phase (liquid and vapor) inclusions (referred to as *Type IIa* inclusions) occur rarely in a cloudy zone within the core of apatite (*Fig. 8c*). Water was detected in the liquid phase along with an indication of CO_2 in the vapor phase (*Fig. 10*).

Slightly elongated, typically negative crystal-shaped, 2–10-μm-sized two-phase (liquid and vapor) fluid inclusions were distinguished along growth zones in apatite, which indicate primary origin. These inclusions are distributed outside the core of apatite, and are referred to as Type IIb inclusions (*Fig. 8c–d*). CO_2 was detected in the vapor phase and H_2O in the liquid phase (*Fig. 10*). Consistent phase ratios were observed (one-phase fluid entrapment).

Apatite, showing intergrowth with chlorite and containing small chlorite and chalcopyrite as inclusions, hosts randomly distributed primary multiphase (solid, liquid and vapor) fluid inclusions as well (referred to as Type IIc inclusions). These inclusions are characterized by negative crystal shape and sizes ranging between 2–8 μm. Chlorite was found as an accidentally trapped solid phase within the inclusions, together with water in the liquid phase and a $CO_2 \pm CH_4$ in the vapor phase (*Fig. 10*). Fluid compositions vary as follows: CO_2: 93–100 mol%, CH_4: 0–7 mol%. Note that apatite, hosting multiphase fluid inclusions, is commonly rich in intracrystalline cracks filled by brown iron-oxide-rich material (*Fig. 8e–f*).

Type IId inclusions in apatite are mostly distributed along healed fractures perpendicular to the elongation of the host mineral (*Fig. 8g, h*). These secondary two-phase (liquid and vapor) fluid inclusions have elongated and irregular shape and 1–15 μm size. Phase ratios vary significantly (from exclusively vapor containing to almost only liquid containing inclusions) within the same healed fracture. CO_2 in the vapor phase and H_2O in the liquid phase were detected (*Fig. 10*).

Calcite occurs as a common vein-filling mineral within the analyzed samples and contains abundant two-phase (liquid and vapor) fluid inclusions, referred to as Type III inclusions. These fluid inclusions occur either in the core or randomly within the calcite grains (*Fig. 9a, b*) thus are pri-

→ **Figure 8.** Photomicrographs showing representative petrographic features of the studied fluid inclusion types in rock-forming minerals of Penninic greenschist samples from the Szh-II (plane polarized, transmitted light). a–b) Secondary CH_4-rich aqueous two-phase fluid inclusions (Type I) occurring in healed fractures in clinozoisite. c–d) Primary fluid inclusion types (Type IIa and b) trapped in apatite. Type IIa inclusions are located in the core of the host apatite in cloudy zone, while Type IIb occur along growth zones outside the core. e–f) Primary multiphase fluid inclusions (Type IIc) hosted by apatite, which has abundant intergranular cracks filled by iron-oxide-rich fine-grained material. Note that the apatite has an intergrowth with chlorite at the grain boundaries. Furthermore, chlorite also occurs as crystal inclusions in apatite and as an accidentally trapped solid phase in the fluid inclusions. g–h) Secondary CO_2-CH_4-rich aqueous fluid inclusion (Type IId) trails in apatite, mostly distributed perpendicular to the elongation of the host mineral. Black rectangles on a), c), e) and g) show the location of close-up views shown on b), d), f) and h) respectively

Abbreviations: Act – actinolite, Chl – chlorite, Qz – quartz, Czo – clinozoisite, Ap – apatite, S – solid phase, L – liquid phase, V – vapor phase

→ ***8. ábra.*** *A Szh-II fúrásból származó Pennini zöldpalaminták kőzetalkotó ásványaiban megfigyelt fluidumzárvány típusok főbb petrográfiai sajátosságai (1N, áteső fény). a–b) Másodlagos CH_4-tartalmú vízgazdag kétfázisú fluidumzárványok (I. típus) klinozoisitben, melyek beforrt repedések mentén jelennek meg. c–d) Elsődleges fluidumzárványok apatitban, melyek a befogadó ásvány magjában felhőszerűen (II.a típus), illetve növekedési zónái mentén (II. b típus) jelennek meg. e–f) Primer multifázisú fluidumzárványok (II.c típus) apatitban. A befogadó ásvány repedésekkel gazdagon átjárt, melyeket vas-oxid(ok)ban gazdag, finomszemcsás anyag tölt ki. Megállapítható, hogy a klorit az apatittal párhuzamosan kristályosodott, ugyanis klorit figyelhető meg az apatit zárványaként, illetve a fluidumzárványokban véletlenszerűen csapdázott szilárd fázisként is. g–h) Másodlagos CO_2-CH_4-tartalmú vízgazdag (II.d típus) fluidumzárványok, melyek apatit beforrt repedései mentén, általában a befogadó ásvány megnyúlására merőlegesen csapdázódtak. Az a), c), e) ábrán jelölt fekete téglalapok rendre a b), d), f) és h) kinagyított képeinek helyét mutatják*

Rövidítések: Act – aktinolit, Chl – klorit, Qz – kvarc, Czo – klinozoisit, Ap – apatit, S – szilárd fázis, L – folyadékfázis, V – gőzfázis

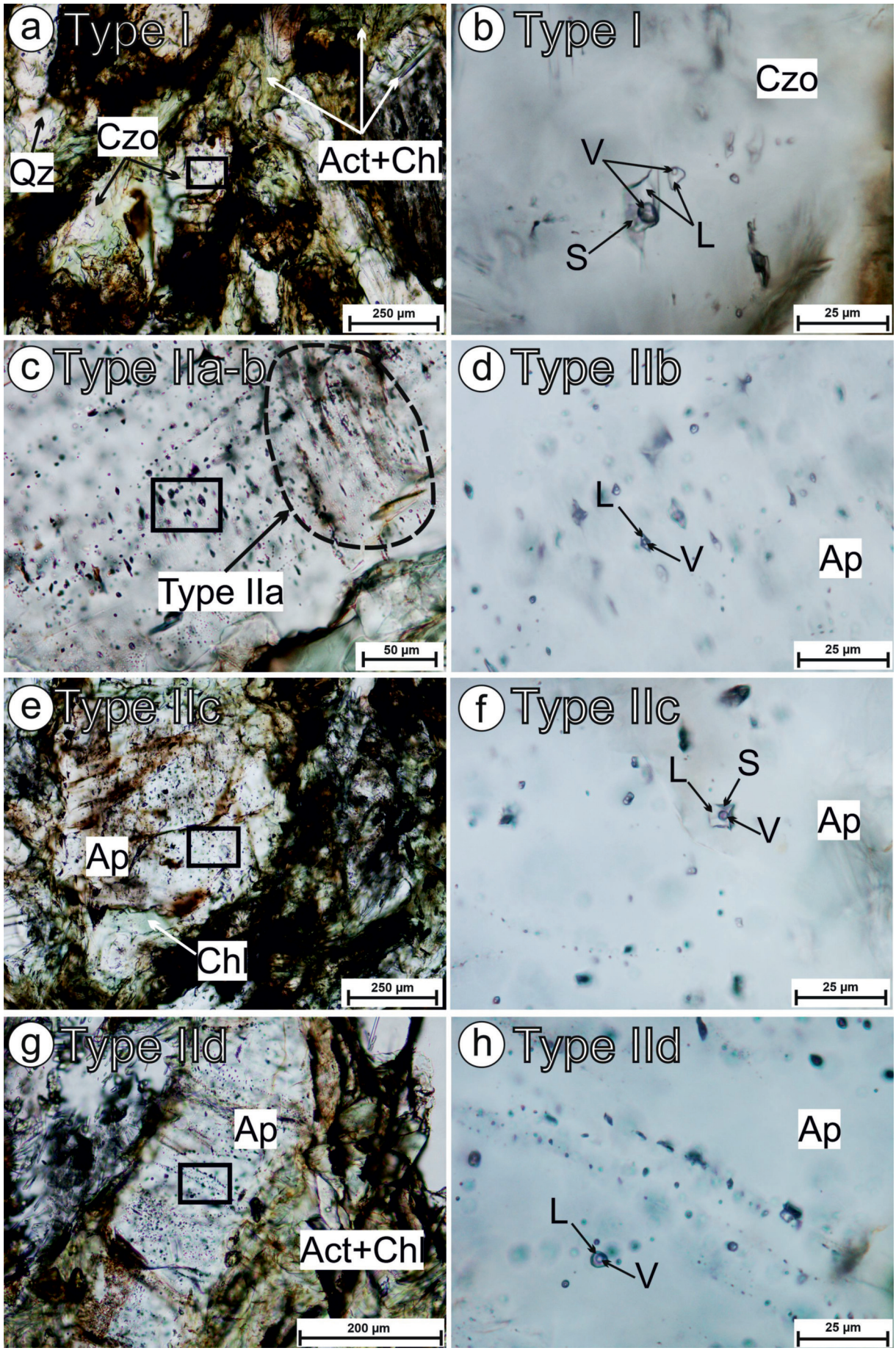
a Type I
Qz
Czo
Act+Chl
250 µm
b Type I
Czo
V
L
S
25 µm
c Type IIa-b
Type IIa
50 µm
d Type IIb
L
V
Ap
25 µm
e Type IIc
Ap
Chl
250 µm
f Type IIc
L
S
V
Ap
25 µm
g Type IId
Ap
Act+Chl
200 µm
h Type IId
Ap
L
V
25 µm

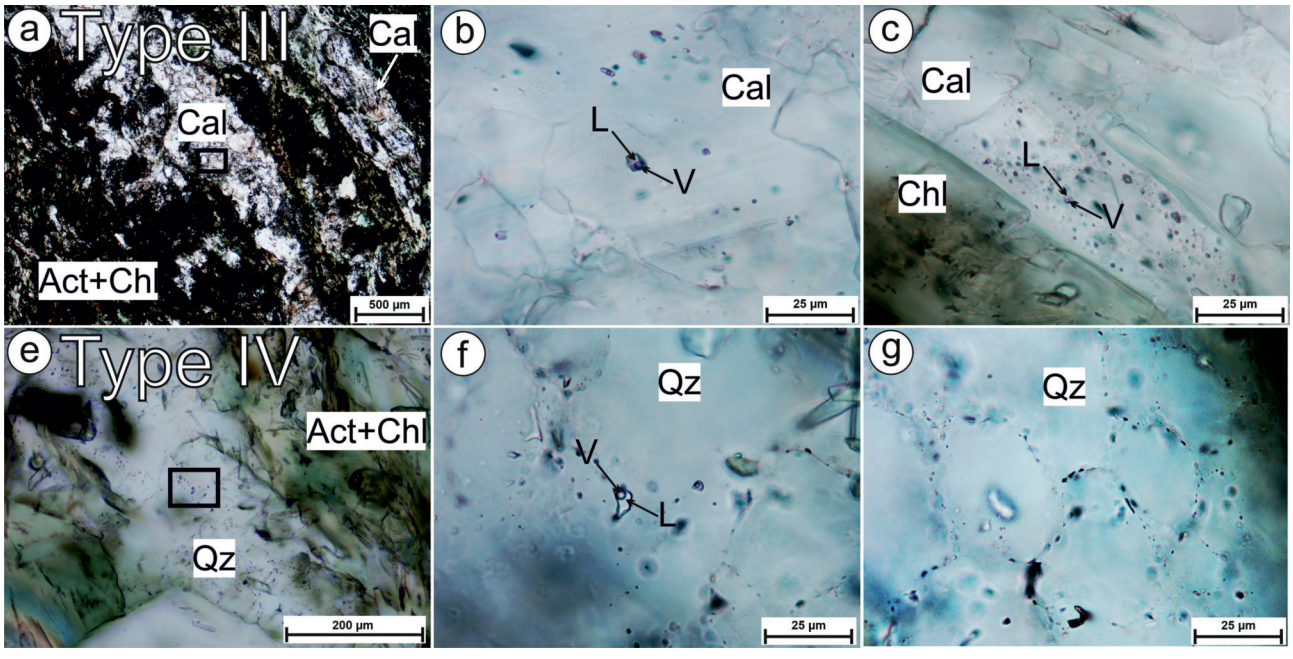

Figure 9. Photomicrographs showing characteristic petrographic features of the studied fluid inclusion types in vein-filling minerals of Penninic greenschist samples from the Szh-II well (plane polarized, transmitted light). a-b) Type III inclusions, hosted by calcite, have primary origin as they occur in the core or randomly in the calcite grains and also distributed parallel to the veins. c-d) Type IV secondary two-phase CO_2-CH_4-N_2-rich aqueous fluid inclusions occurring along subgrain boundaries of vein-forming quartz. Black rectangles on a) and e) show the location of close-up views shown on c) and f), respectively
Abbreviations: Act – actinolite, Chl – chlorite, Qz – quartz, Cal – calcite, L – liquid phase, V – vapor phase

9. ábra. *A Szh-II fúrásból származó Pennini zöldpalaminták érkitöltő ásványaiban megfigyelt fluidumzárvány típusok főbb petrográfiai sajátosságai (1N, áteső fény). a-b) Elsődleges fluidumzárványok kalcitban, melyek a szemcsék magjában vagy véletlenszerű eloszlásban, továbbá az erek lefutásával párhuzamosan jelennek meg. c-d) Másodlagos, kétfázisú CO_2-CH_4-N_2-tartalmú, vízgazdag fluidumzárványok, melyek érkitöltő kvarc alszemcse határai mentén helyezkednek el. Az a), e) ábrán jelölt fekete téglalapok rendre a c) és d) kinagyított képeinek helyét mutatják*
Rövidítések: Act - aktinolit, Chl - klorit, Qz - kvarc, Cal - kalcit, L - folyadék fázis, V - gőz fázis

mary in origin. Calcite veins less typically host small (< 2-µm-sized) fluid inclusions with a distribution outlining the direction of the vein without following any straight healed fracture (*Fig. 9c*). This textural observation indicates primary entrapment of the fluid inclusions most likely simultaneously with vein formation. Type III inclusions are 1–5-µm-sized with elongated-irregular, in some cases nearly negative crystal shape. Although the inclusions are almost always two-phase, their phase ratios show strong variations with one phase liquid or vapor inclusion end members present within the same cluster. H_2O was detected in the liquid phase, while CO_2, in addition to indication of saturated hydrocarbons, in the vapor phase (*Fig. 10*). The presence of saturated hydrocarbons is indicated by low intensity broad Raman bands at ~2250 cm^{-1} and ~2945 cm^{-1}, based on LI et al. (2023) and ZHANG et al. (2007). Despite the high intensity baseline of the Raman spectra caused by the host calcite (and thus low signal-to-noise ratio), these two bands were detected in some of the studied inclusions. This observation is consistent with the findings of LI et al. (2023) describing the main Raman bands of saturated hydrocarbons in the same host mineral.

Quartz-rich veins, which are less common than calcite-veins, contain sparse and tiny (typically <1–2 µm, very rarely reaching 5–6 µm sized) fluid inclusions, referred to as Type IV inclusions along quartz subgrains (*Fig. 9e–g*). These two-phase (liquid and vapor) inclusions have irregular shape. The low visibility due to the small size precluded estimating possible variations of phase ratios. Raman spectroscopy revealed the co-existence of CO_2, CH_4 and N_2 in the vapor phase and H_2O in the liquid phase (*Fig. 10*). These inclusions are defined as secondary fluid inclusions encapsulating fluids during quartz subgrain formation.

Discussion and outlook for future work

Structural interpretation

In most detachment systems, brittle (cataclastic) deformation during fault slip overprints a high-strain ductile shear zone made of mylonites. This might be the consequence of the embrittlement of the shear zone related to extensional unroofing (exhumation and cooling) or the injection of fluids into the shear zone (*Fig. 6*; REYNOLDS & LISTER 1990, GAUTIER & BRUN 1994, BRUN et al. 1994, SELVERSTONE et al. 2012, WHITNEY et al. 2013, AXEN 2019).

The greenschists in the Szh-II drill core exhibit signs of minor to moderate ductile shearing under greenschist facies conditions (*Fig. 6b*), associated with a downdip stretching lineation and shear sense based on observed stretching lineations and asymmetric folds. These observations are consistent with earlier findings that describe the youngest, dominant metamorphic event in the Rechnitz MCC as the

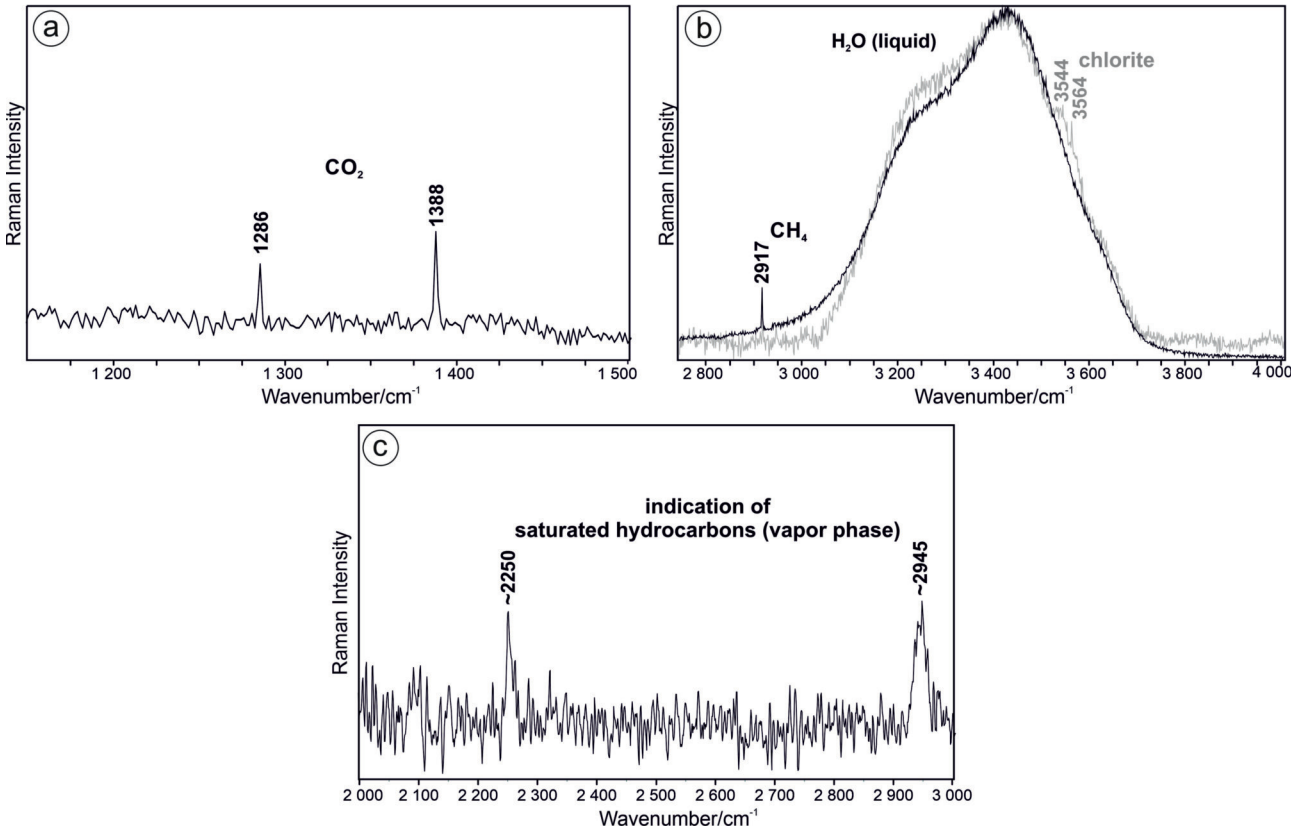

Figure 10. Representative Raman spectra of the most common fluid components measured in fluid inclusions of greenschist samples. a) Characteristic Raman spectra of CO_2 measured in the vapor phase of in Type IIa-d, III and IV fluid inclusions. b) Characteristic Raman spectra of CH_4 and H_2O detected in the vapor and liquid phase of fluid inclusions, respectively. CH_4 was detected in Type I, Type IIc and Type IV inclusions, whereas liquid H_2O in each fluid inclusion type. Raman spectra with grey color indicate the overlapping OH bands of accidentally trapped chlorite measured in Type IIc inclusions. c) Raman spectra showing the indication of saturated hydrocarbons detected in calcite-hosted Type III fluid inclusions

10. ábra. *A zöldpalamintákban vizsgált fluidumzárvány típusok legfőbb fluidumkomponenseinek jellegzetes Raman-spektrumai. a) A II.a-d, II.I és IV. típusú fluidumzárványok gőzfázisában megfigyelhető CO_2 Raman-spektruma. b) Az I., II.c és IV. típusú típusú fluidumzárványok gőzfázisában mért CH_4 és folyadékfázisában mért H_2O, mely utóbbi az összes zárványtípusban kimutatható. Megfigyelhetők továbbá a szürke színnel jelzett Raman-spektrumon a H_2O spektrumával részben átfedő klorit jellegzetes Raman-sávjai, mely utóbbi a II.c típusban véletlenszerűen befogott szilárd fázisként azonosítható. c) Telített szénhidrogének jelenlétét indikáló Raman-spektrum, mely a III. típusú halcit által bezárt fluidumzárványokban mutatható ki*

formation of the greenschist fabric, associated with E–NE-vergent shearing (Lelkes-Felvári 1982, 1994; Kubovics 1983; Koller 1985; Cao et al. 2013). While high strain rate shear zones have been reported from the wider Rechnitz complex (Cao et al. 2013), mylonites with significant grain size reduction have not been observed in the samples of the Szh-II drill core. This suggests that this specific portion of the Penninic unit was not in proximity (i.e. within a few hundred meters) of the main ductile shear zone during the formation of the detachment system (*Fig. 11a*). Instead, these samples might represent a distal section of exhumed rock volume with respect to the main ductile shear zone, which was crosscut by a younger fault of the detachment system once already cooled below the limit of ductile deformation (*Fig. 11b*). However, the observed deformation features (*Fig. 6b*) still indicate a moderate degree of ductile deformation that could be related to shearing during initial exhumation, not directly adjacent to a main shear zone. This possibility is supported by the overall 20–40° dip of the foliation, which is similar to the low-angle dip of the detachment fault seen on reflection seismic data (*Fig. 1b*). However, we note that any robust interpretation would require oriented samples (allowing to constrain the dip direction as well), which were not available for the cores of this study.

We emphasize that the above-described deformation zone directly underlies the syn-rift conglomerates. In this sense, the SW-Danube Basin may be interpreted genetically as a supra-detachment basin, and the Paleozoic slivers in the uppermost 20 meters of the basement might represent an extensional allochthon that is bounded by different branches of the main detachment.

Stratigraphic interpretation

Our analysis of the core material from the Szh-II well associated with Miocene normal faulting highlighted several interpretational challenges. One of them is the stratigraphic nature of the various Upper Austroalpine unit lithologies in the broader damage zone of the Rechnitz fault between about 2063–2083 m (*Figs 2b, 3*). Lelkes-Felvári (1994) likened these lithologies to those in the Graz Paleozoic, some 150 km to the west. In our view, a more straightforward

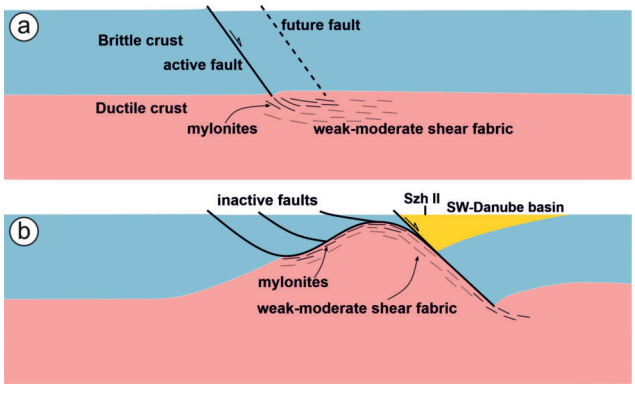

Figure 11. Schematic evolutionary model (rolling-hinge model) of the Rechnitz detachment system, where the major fault penetrated by the Szh-II well is the youngest fault of the detachment system. This could explain why the fault is directly underlain by weakly-moderately sheared Penninic greenschists and not by well-developed mylonites. a) Initial extension: formation of the first fault(s) in the brittle crust and a shear zone in the ductile crust. b) Exhumation of the metamorphic core complex (Rechnitz window) while the active faulting migrates from left to right

11. ábra. *A Rohonci nyírózóna sematikus fejlődéstörténeti rekonstrukciója, melyben a Szh-II fúrás a rendszer legfiatalabb vetőjét harántolta. Ez szolgálhat magyarázatul arra, hogy közvetlenül a vető alatt elhelyezkedő Pennini zöldpala csak kis-közepes mértékű nyírást szenvedett, illetve milonitosodás jeleit nem mutatja. a) Extenzió kezdete: a kéreg ridegen deformálódó zónájában az első vető(k), a képlékeny alsó kéregben pedig nyírózóna kialakulása. b) A metamorf magkomplexum (Rohonci-ablak) exhumációja, melynél az aktív vetők balról jobbra tevődnek át*

correlation is one with the Devonian units exposed in the active quarry near Hannersdorf, only about 15 km to the west (*Fig. 1a*). The phyllites and dolomites (*Fig. 12*) described at this location (SCHÖNLAUB 2000) are very likely the equivalents of the Ölbö Carbonate phyllite and Bük Dolomite formations documented in the subsurface of the southwestern Danube Basin (FÜLÖP 1990).

The lack of any Lower and Middle Austroalpine lithologies in the damage zone and in the overlying fault talus highlights the large normal offset along the Rechnitz fault displacing about a 10 km thick section of mostly high-grade metamorphics (TARI 1996b). However, a well-developed mylonite zone in the footwall greenschists, which would be expected to be associated with such a high-strain fault (AXEN 2019), was not found in the Szh-II drill core. In our interpretation, it is attributed to the brittle overprint of the detachment fault in a later stage of the extension (*Fig. 6b*). This portion of the Penninic unit was likely not in the proximity (i.e., within few hundred meters) of the main ductile shear zone. In a map-view sense, the middle Miocene low-angle faults developed with a dominant down to the SE sense, almost perpendicular to the top to the ENE movement during the early Miocene MCC style faulting. Therefore, the subsurface boundary of the Rechnitz Window may be a composite one, i.e., a combination of high-strain detachment and wide-rift style low-angle normal fault segments (*Fig. 1a*). Given the limited subsurface seismic reflection and well control (TARI et al. 2020), the map which has been strongly modified from KRÖLL et al. (1988), remains speculative (*Fig. 1a*).

Importantly, during the late Miocene and Pliocene (12.5–5.5 Ma, Sarmatian–Lower Pannonian) the Rechnitz fault plane is inferred to have experienced a fault reactivation period (KOVÁCS et al. 2015). Therefore, the fault zone may have recorded at least three distinct faulting episodes. There are multiple generations of cement seen in the damage zone (*Figs 3, 4*), but their chronology cannot be tied at present to the distinct brittle deformation stages along the Rechnitz fault. A more detailed structural analysis than what our study offers may result in a more specific chronology of diagenetic sequence as the function of fault reactivation.

Migration of fluids along the fault zone

The fact that gases occluded in fracture zones of active faults are characterized by a high concentration of H_2 and/or CO_2 has been known for decades (SUGISAKI et al. 1983). The

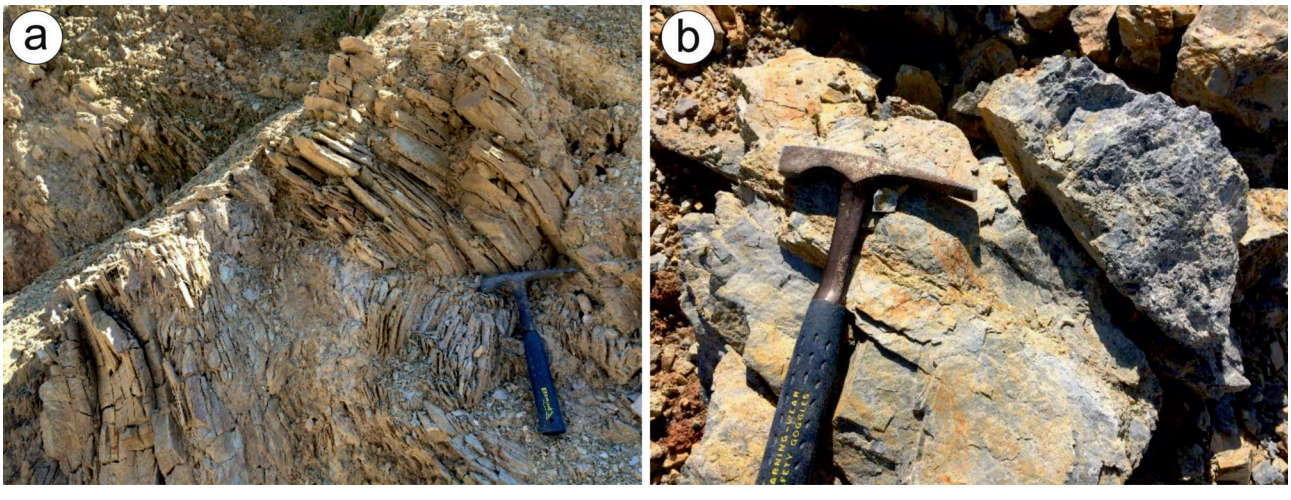

Figure 12. Outcrop expression of Upper Austroalpine a) slates-phyllites and b) dolomites in an active quarry just south of Hannersdorf (*Fig. 1a*). These Devonian lithologies are tentatively correlated with the fractured material observed in the inferred damage zone of the Rechnitz fault between 2063-2085 m in the Szh-II well (*Fig. 2b*)

12. ábra. *A Felső Ausztroalpi egységek (a: fillit, b: dolomit) feltárásai a Hannersdorftól (Ausztria,* 1. ábra, a*) délre található aktív kőfejtőben. Ezek a devon időszaki kőzettani egységek párhuzamosíthatók legjobban a vizsgált fúrásanyag (*2. ábra, b*) leginkább töredezett, deformált zónájában (2063-2085 m) vizsgált kőzetekkel*

concentration of H_2, in particular, in active faults associated with historical earthquakes usually amounts to as high as several percent at most, whereas the concentration of H_2 from Quaternary faults that have not been shown to produce historical earthquakes is at most 100 ppm.

Upward migration of gases in a fault damage zone requires some porosity and permeability. Neotectonic faults tend to allow these as diagenetic processes has not had sufficient time yet to plug the pore spaces. Existing brittle fault evolution models assume a cyclic permeability evolution of fault zones through geological time (INDREVÆR et al. 2014). With ongoing faulting, movement along a fault causes fracturing and cataclasis within the core zone and increases permeability. The core zone thereby acts as a fluid conduit (*Fig. 13a*). However, cementation by precipitation of minerals and grain growth decreases permeability within the core zone and forces the gas and fluid flow into the adjacent damage zones flanking the plugged-up fault (*Fig. 13b*). Only fault reactivation could initiate a new fluid flow evolution cycle by opening up the core fault zone by brittle deformation (PEI et al. 2015).

Fluid evolution history

Four different types of fluid inclusions representing different fluid migration events were distinguished in the studied rocks, as follows: Type I: CH_4–H_2O fluid, Type II: CO_2±CH_4–H_2O fluid, Type III: CO_2–H_2O±hydrocarbon fluid and Type IV: CH_4–CO_2–N_2–H_2O fluid. CH_4–CO_2–N_2 aqueous fluids are common in fluid inclusions trapped during retrograde hydration under greenschist facies conditions and along a retrograde metamorphic path in exhumed rocks (VAN DEN KERKHOF et al. 1991).

A precise chronological classification for Type I and Type IId inclusions is challenging to be established as they occur in healed fractures of rock-forming minerals, thus entrapped subsequently to crystallization of the host minerals. Apatite hosts primary fluid inclusions within its core (Type IIa inclusions) and along growth zones (Type IIb-c inclusions), thus representing different stages of entrapment. Original magmatic signatures in the core zone of apatite are commonly preserved in low-grade metamorphic rocks (HENRICHS et al. 2019), whereas metamorphic overgrowth of apatite forms due to partial dissolution-recrystallization processes (SPEAR & PYLE 2002). Type IIa inclusions are thus most likely representatives of an ancient fluid generation characterized by primary magmatic origin, although subsequently underwent stretching and partial opening/decrepitation over a metamorphic P–T path. Textural evidence indicates that metamorphic apatite crystallization took place in the presence of chlorite as the latter was found as an accidentally trapped phase in the inclusions. This suggests that apatite grew in the presence of a H_2O–CO_2 fluid which was

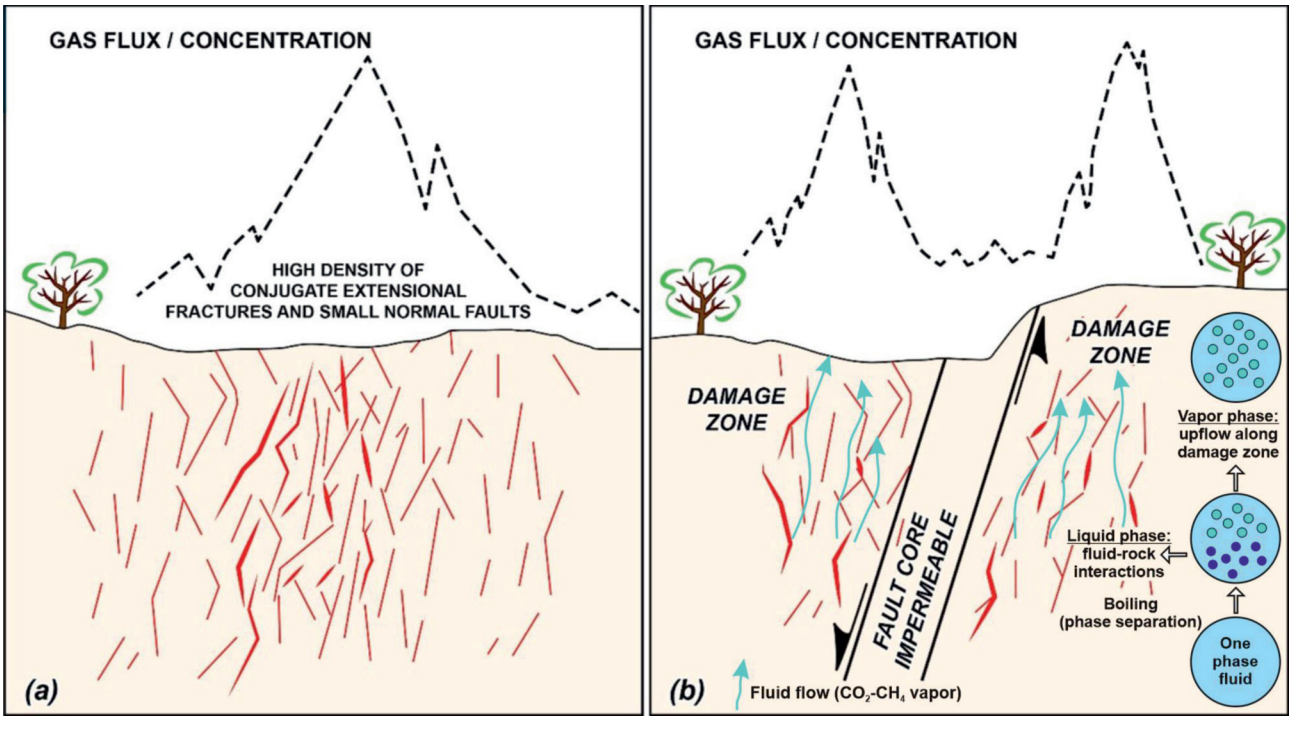

Figure 13. Schematic depiction of how gas leakage along a brittle fault could evolve through time, modified from ANNUNZIATELLIS et al. (2008). a) The fault network configuration results in more open, interconnected gas migration pathways, resulting in higher gas flux rates. b) The mature fault shows the development of a very low permeability core, bounded by damage zones that could become the actual migration pathways for vapors or liquids until the fault zone reactivates (INDREVÆR et al. 2014, PEI et al. 2015)

13. ábra. *Fluidumáramlás/gázszivárgás időbeli fejlődése egy rideg deformációs zónában, sematikus ábrázolás ANNUNZIATELLIS et al. (2008) alapján. a) A vetőrendszer jellege nyitottabb, egymással kommunikáló fluidum/gáz migrációs útvonalakat eredményez, ezzel elősegítve az intenzív áramlást. b) A vetőrendszer későbbi fejlődési szakaszában annak belső zónája impermeábilissá válhat, így az azt körülvevő deformált zónák jelölhetik ki a fluidum feláramlási útvonalakat a vetők reaktiválásáig (INDREVÆR et al. 2014, PEI et al. 2015)*

preserved as primary CO_2-bearing aqueous inclusions (Type IIb). Apatite was crosscut by abundant cracks filled by iron-oxide-rich fine-grained material, developed probably during retrograde evolution. This likely resulted in partial opening of primary fluid inclusions (Type IIc) which could cause COH fluid re-speciation via redox reactions (CONOLLY 1993, CESARE 1995). Such open system fluid compositional modifications causing post-entrapment re-equilibration of inclusions might took place locally that is supported by variations of the molar volume of CO_2 and CH_4 within the same assemblage of inclusions occurring close to cracks and fractures. Re-speciation of the fluid and redox reaction within inclusions can be influenced by H_2O leakage or hydrogen diffusion into or out of the inclusion (HUIZENGA 2001). Such enrichment of CH_4 can be described by the following reaction:

$$CO_2 + 4H_2 = CH_4 + 2H_2O$$

This reaction takes place typically during serpentinization of ultramafic rocks along with continuous production of H_2 and decrease of H_2O activity (KLEIN et al. 2019). Serpentinization of ultramafic rocks within the Penninic unit (DUNKL & DEMÉNY 1997) could have served as a source for hydrogen production. However, we have no direct evidence for the presence of the H_2 in the studied fluid inclusions. Alternatively, the source of various COH fluids (i.e., CO_2 and CH_4 as found in apatite-hosted fluid inclusions) could have been organic matter, which likely produced hydrocarbons, as detected in Type III inclusions.

Textural data showed that Type IId secondary fluid inclusions clearly postdate the development of the abovementioned fluid inclusion generations and are characterized by heterogeneous trapping and a boiling system during entrapment indicated by varying liquid-vapor ratios within the same healed fracture.

Based on textural analyses, the entrapment of Type III and Type IV inclusions are related to the enclosing calcite and quartz veins, respectively. Type IV carbonic nitrogen-bearing aqueous inclusions distributed along quartz subgrain boundaries are likely to have been trapped during ductile deformation-recrystallization processes (JOHNSON & HOLLISTER 1995). Type III inclusions with primary origin, which are included in calcite veins that mostly occur along post-foliation fractures with high angle with respect to foliation, can be regarded as the latest fluid migration event recorded by the studied greenschist samples.

As an alternative scenario, necking-down phenomenon as a possible post-trapping change of fluid inclusions cannot be excluded in particular for fluid inclusions trapped in soft minerals, such as calcite. However, a thorough petrographic analysis of fluid inclusions can help to recognize the peculiarities caused by necking-down, as described by GOLDSTEIN (2001). Based on these, we did not find such petrographic evidence like i.e., 1) left-over tails or channels or 2) paired gas-rich and liquid-rich inclusions, rather randomly distributed inclusions in terms of their phase ratios (GOLDSTEIN & REYNOLDS 1994). Furthermore, if a typical aqueous liquid is entrapped homogeneously at higher temperatures, it is only able to nucleate a vapor bubble upon cooling that would occupy no more than 15% of the volume of the inclusion (GOLDSTEIN, 2001). Consequently, if within a group of fluid inclusions, there is more than 15 vol.% vapor, then heterogeneous entrapment of a gas and liquid phase is likely, which fits our observations in this study.

Regardless of the fluid inclusions type, all inclusions indicate liquid/vapor phase separation during upward fluid migration through some channel, i.e., the fault network. A clear manifestation of this is the co-existence of vapor and liquid phases within the inclusions during (Type IId and Type III) or after (Type I, Type IIa–c) fluid entrapment as inclusions. This can be of particular importance when considering the migration of the various fluid generations. Composition of phases defined by Raman spectroscopy and phase topology of CO_2–H_2O (DIAMOND 2001) and CH_4–H_2O (DUAN et al. 1992) suggest that during liquid-vapor phase separation, a H_2O-rich liquid and a CO_2- or CH_4-rich vapor phase will be immiscible during the upward flow of fluids (by decreasing pressure and/or temperature). Once the liquid and the vapor rich phases form, they likely physically separate from each other due to their different physicochemical properties and flow abilities. The H_2O-rich fluid will likely play a role in dissolution/precipitation and metasomatic processes with their environment (rocks) due to its high solvation capacity. In contrast, the more inert and low-density CO_2 and CH_4 vapor would probably flow through the damage zones (see *Fig. 13*), reaching the shallow subsurface region or even the atmosphere.

Our thin section analysis and macroscopic observations show that the Rechnitz fault is probably "tight" as pre-existing pore-space created by successive brittle faulting periods is filled with calcite and/or quartz cement today. There is no structural evidence for neotectonic activity along the Szh-II fault (KOROKNAI et al. 2020). Existing earthquake data in the region do not support recent reactivation of the fault either (CZECZE et al. 2023). Therefore, the cemented Rechnitz fault core zone may not be preferentially used by various gases and fluids to migrate towards the surface at present.

Yet, the three fluid inclusion samples taken from the footwall of the Rechnitz fault indicate migration of gases, such CH_4 or CO_2, along the fault in the past. Additional fluid inclusion work on samples from the broader damage zone may possibly document the paleo-migration of other gases and fluids as well.

Conclusions

The fully cored Szh-II well offers an exceptional case where a major fault zone was penetrated in its entire 15–20-m-thick damage zone immediately beneath the syn-rift Miocene basin fill. The highly fragmented Paleozoic slates, phyllites and carbonates are correlated with Upper Austroalpine Devonian lithologies outcropping only about 15 km to the west near Hannersdorf, Austria. The brittle fault dam-

age zone may have some extensional allochthons associated with the high-strain (tens of kilometers) Miocene extensional movements along the Rechnitz-Rohonc fault complex.

However, no mylonitic fabric was found corresponding to the expected mylonitic front in the cores beneath the fault in its footwall. Instead, it is the Miocene to Pliocene brittle deformation that dominates the deformation style as revealed by the cores recovered at the well location.

Different diagenetic events were documented in the Upper Austroalpine (UAA) Paleozoic and Penninic units; however, a single paragenetic sequence cannot be formulated at this time. The pervasive cementation events (silica and carbonate) occluded the pore space entirely in all analyzed samples. Silica cements and silica replacement were found only in the UAA limestone, interpreted as potentially hydrothermal in origin. However, initial porosity that existed before the cementation was revealed by thin section analysis. This porosity developed due to fracturing within the detachment zone.

Even though the Rechnitz/Rohonc fault zone is presently tight due to the cementation episodes, fluid inclusion analysis on three greenschist samples in the footwall of the fault suggests paleo-migration of gases, including CH_4 or CO_2. Four major fluid migration events were distinguished as follows: Type I: CH_4–H_2O fluid, Type II: CO_2±CH_4–H_2O fluid, Type III: CO_2–H_2O±hydrocarbon fluid and Type IV: CH_4–CO_2–N_2–H_2O fluid. All fluid generations indicate, however, that liquid-vapor phase separation took place during upward fluid migration. The separation of fluid components strongly supports the upward flow of low-density vapor (i.e., CO_2 or CH_4) through damage zones of fault networks.

The relatively low number of samples analyzed in this study leaves room for a more detailed structural and petrographic study of the fully cored Szh-II well. However, the preliminary results of this study suggest that this particular well that penetrates the Rechnitz/Rohonc fault zone may not serve as a simple generic analogue for other major detachment faults in the broader Pannonian Basin system.

Acknowledgements

We are pleased to thank Prof. Csaba Szabó for all the knowledge we learned from him regarding petrology and geochemistry during our university years. With this manuscript and the enclosing special issue, we aim to pay our great tribute to Prof. Csaba Szabó's lifelong mentoring and teaching activity, during which he created the Lithosphere Fluid Research Laboratory. Professor Szabó has carried out outstanding human-centered professional education and research training that transcends its age and environment. P. Pernegr kindly drafted some of the figures. M. Berkesi, T. Spránitz and K. Porkoláb acknowledge the funding from MTA-EPSS FluidsByDepth Research Group (LP2022-2/2022). M. Berkesi and T. Spránitz were partially supported by NKFIH_FK research funding number 132418.

References – Irodalom

Annunziatellis, A., Beaubien, S. E., Bigi, S., Ciotoli, G., Coltella, M. & Lombardi, S. 2008: Gas migration along fault systems and through the vadose zone in the Latera caldera (central Italy): Implications for CO_2 geological storage. – *International journal of greenhouse gas control* **2/3,** 353–372. https://doi.org/10.1016/j.ijggc.2008.02.003

Aubert, I., Lamarche, J. & Léonide, P. 2021: Ternary fault permeability diagram: An innovative way to estimate fault zones hydraulics. – *Journal of Structural Geology* **147,** p.104349. https://doi.org/10.1016/j.jsg.2021.104349

Aubert, I., Lamarche, J., Richard, P. & Leonide, P. 2022: Imbricated structure and hydraulic path induced by strike slip reactivation of a normal fault. – *Journal of Structural Geology* **162,** p.104702. https://doi.org/10.1016/j.jsg.2022.104702

Axen, G. J. 2019: How a strong low-angle normal fault formed: The Whipple detachment, southeastern California. – *Geological Society of America Bulletin* **132/9–10,** 1817–1828. https://doi.org/10.1130/b35386.1

Bernal, A. J. 2024: Fault-seal analysis in the Greater Bay du Nord area, Flemish Pass Basin, offshore Newfoundland. – *Petroleum Geoscience* **30/1**. https://doi.org/10.1144/petgeo2023-019

Brun, J. P., Sokoutis, D. & Vandendriessche J. 1994: Analog Modeling of Detachment Fault Systems and Core Complexes. – *Geology* **22/4,** 319–322. https://doi.org/10.1130/0091-7613(1994)022%3C0319:amodfs%3E2.3.co;2

Cao, S., Neubauer, F., Bernroider, M., Liu, J. & Genser, J. 2013: Structures, microfabrics and textures of the Cordilleran-type Rechnitz metamorphic core complex, Eastern Alps. – *Tectonophysics* **608,** 1201–1225. https://doi.org/10.1016/j.tecto.2013.06.025

Cesare, B. 1995: Graphite precipitation in C–O–H fluid inclusions: closed system compositional and density changes, and thermobarometric implications. – *Contributions to Mineralogy and Petrology* **122/1–2,** 25–33. https://doi.org/10.1007/s004100050110

Connolly, J. A. D. & Cesare, B. 1993: C–O–H–S fluid composition and oxygen fugacity in graphitic metapelites. – *Journal of Metamorphic Geology* **11,** 379–388. https://doi.org/10.1111/j.1525-1314.1993.tb00155.x

Czecze B., Győri E., Timkó M., Kiszely M., Süle B. & Wéber Z. 2023: A Kárpát–Pannon régió szeizmicitása: aktualizált és átdolgozott földrengés-adatbázis. – *Földtani Közlöny* **153/4,** 279–295. https://doi.org/10.23928/foldt.kozl.2023.153.4.279

Diamond, L. W. 2001: Review of the systematics of CO_2–H_2O fluid inclusions. – *Lithos* **55,** 69–99. https://doi.org/10.1016/S0024-4937(00)00039-6

Duan, Z., Moller, N. & Weare, J. H. 1992: An equation of state for the CH_4–CO_2–H_2O system: II. Mixtures from 50 to 1000 °C and 0 to 1000 bar. – *Geochimica et Cosmochimica Acta* **56,** 2619–2631. https://doi.org/10.1016/0016-7037(92)90348-m

Demény, A. & Dunkl, I. 1991: Preliminary zircon fission track results in the Kőszeg Penninic unit, W. Hungary. – *Acta Mineralogica-Petrographica* **32,** 43–47.

Dubessy, J., Poty, B. & Ramboz, C. 1989: Advances in COHNS fluid geochemistry based on micro-Raman spectrometric analysis of fluid inclusions. – *European journal of Mineralogy* **1/4,** 517–534. https://doi.org/10.1127/ejm/1/4/0517

Dunkl, I. 1992: Final episodes of the cooling history of eastern termination of the Alps. – In: Neubauer, F. (ed.): *The Eastern Central Alps of Austria: ALCAPA 1992 meeting field guidebook*, 137–139.

Dunkl, I. & Demény, A. 1997: Exhumation of the Rechnitz Window at the border of Eastern Alps and Pannonian basin during Neogene extension. – *Tectonophysics* **272,** 197–211. https://doi.org/10.1016/S0040-1951(96)00258-2

Frezzotti, M. L., Tecce, F. & Casagli, A. 2012: Raman spectroscopy for fluid inclusion analysis. – *Journal of Geochemical Exploration* **112,** 1–20. https://doi.org/10.1016/j.gexplo.2011.09.009

Fülöp, J. 1990: *Geology of Hungary, Paleozoic I.* – MÁFI, Budapest, 326 p. (in Hungarian)

Goldstein, R. H. 2001: Fluid inclusions in sedimentary and diagenetic systems. – *Lithos* **55/1–4,** 159–193. https://doi.org/10.1016/S0024-4937(00)00044-X

Goldstein, R. & Reynolds, J. (1994): Systematics of fluid inclusions. – *SEPM short course notes* **31,** 213 p.

Gautier, P. & Brun, J.-P. 1994: Crustal-scale geometry and kinematics of late-orogenic extension in the central Aegean (Cyclades and Ewia Island). – *Tectonophysics* **238/1–4,** 399–424. https://doi.org/10.1016/0040-1951(94)90066-3

Haines, T. J., Michie, E. A. H., Neilson, J. E. & Healy, D. 2016: Permeability evolution across carbonate hosted normal fault zones. – *Marine and Petroleum Geology* **72,** 62–82. https://doi.org/10.1016/j.marpetgeo.2016.01.008

Henrichs, I. A., Chew, D. M., O'Sullivan, G. J., Mark, C., McKenna, C. & Guyett, P. 2019: Trace element (Mn–Sr–Y–Th–REE) and U–Pb isotope systematics of metapelitic apatite during progressive greenschist- to amphibolite-facies Barrovian metamorphism. – *Geochemistry, Geophysics, Geosystems* **20/8,** 4103–4129. https://doi.org/10.1029/2019gc008359

Horváth, F. 1993: Towards a mechanical model for the formation of the Pannonian basin. –*Tectonophysics* **226/1–4,** 333–357. https://doi.org/10.1016/0040-1951(93)90126-5

Huizenga, J. M. 2001: Thermodynamic modelling of C–O–H fluids. – *Lithos* **55/1–4,** 101–114. https://doi.org/10.1016/s0024-4937(00)00040-2

Indrevær, K., Stunitz, H. & Bergh, S. G. 2014: On Palaeozoic–Mesozoic brittle normal faults along the SW Barents Sea margin: fault processes and implications for basement permeability and margin evolution. – *Journal of the Geological Society* **171/6,** 831–846. https://doi.org/10.1144/jgs2014-018

Johnson, E. L. & Hollister, L. S. 1995: Syndeformational fluid trapping in quartz: determining the pressure-temperature conditions of deformation from fluid inclusions and the formation of pure CO_2 fluid inclusions during grain-boundary migration. – *Journal of Metamorphic Geology* **13/2,** 239–249. https://doi.org/10.1111/j.1525-1314.1995.tb00216.x

Klein, F., Grozeva, N. G. & Seewald, J. S. 2019: Abiotic methane synthesis and serpentinization in olivine-hosted fluid inclusions. – *Proceedings of the National Academy of Sciences* **116/36,** 17666–17672. https://doi.org/10.1073/pnas.1907871116

Koroknai, B., Wórum, G., Tóth, T., Koroknai, Z., Fekete-Németh, V. & Kovács, G. 2020: Geological deformations in the Pannonian Basin during the neotectonic phase: New insights from the latest regional mapping in Hungary. – *Earth-Science Reviews* **211,** 103411. https://doi.org/10.1016/j.earscirev.2020.103411

Kovács, G., Fodor, L., Kövér, S., Molnár, G., Raab, D., Telbisz, T. & Timár, G. 2015: Verification of Late Miocene to Quaternary structural control on landforms: A case study with comprehensive methodology from a low hilly area (western Pannonian Basin): Austrian. – *Journal of Earth Sciences* **108,** 82–104. https://doi.org/10.17738/ajes.2015.0015

Kovács, Z. (ed.) 2018: *Hydrocarbons in Hungary: Results and opportunities.* – Budapest, Hungary, Hungarian Energy and Public Utility Regulatory Authority, 330 p.

Kröll, A., Flügel, H. W., Seiberl, W., Weber, F., Walach, G. & Zych D. 1988: *Erläuterungen zu den Karten über den steirischen Beckens und der südburgenlandischen Schwelle*. – Geologische Bundesanstalt, Vienna, 47 p.

Lafuente, B., Downs, R. T., Yang, H., Stone, N., Armbruster, T. & Danisi, R. M. 2015: The power of databases: the RRUFF project. – *Highlights in mineralogical crystallography* **1,** 25. https://doi.org/10.1515/9783110417104-003

Lelkes-Felvári, G. 1994: Penninic and Upper Austroalpine Units (Paleozoic of Graz) in the borehole Szombathely-II (Western Hungary). – In: Lobitzer, H. et al. (eds): *Jubiläumsschrift 20 Jahre Geologische Zusammenarbeit Österreich–Ungarn*, Geologische Bundesanstalt, Wien, 379–382.

Li, Yx., Wu, Yw., Guan, R., Yan, Xy 2023: Laser Raman Characteristics of Fluid Inclusions in Chang 7 Shale of Yanchang Formation in Xiasiwan Exploration Area. – In: Lin, J. (ed.) *Proceedings of the International Field Exploration and Development Conference 2022*. IFEDC 2022. Springer Series in Geomechanics and Geoengineering. Springer, Singapore. https://doi.org/10.1007/978-981-99-1964-2_93

Pahr, A. 1977: Ein neuer Beitrag zur Geologie des Nordostsporns der Zentralalpen. – *Verhandlungen Geologische Bundesanstalt* **2,** 23–33.

Pahr, A. 1980: Die Fenster von Rechnitz, Berstein und Möltern. – In: Oberhauser, R. (ed.): *Der Geologische Aufbau Österreichs*. Springer, 320–326.

Palcsu, L., Vető, I., Futó, I., Vodila, G., Papp, L. & Major, Z. 2014: In-reservoir mixing of mantle-derived CO_2 and metasedimentary CH_4–N_2 fluids – Noble gas and stable isotope study of two multistacked fields (Pannonian Basin System, W-Hungary). – *Marine and Petroleum Geology* **54,** 216–227. https://doi.org/10.1016/j.marpetgeo.2014.03.013

Pei, Y., Paton, D. A., Knipe, R. J. & Wu, K. 2015: A review of fault sealing behaviour and its evaluation in siliciclastic rocks. – *Earth-Science Reviews* **150,** 121–138. https://doi.org/10.1016/j.earscirev.2015.07.011

Phillips, R. L., Jámbor, Á. & Révész I. 1992: Depositional environments and facies in continuous core from the Szombathely-II well (0-2150 m), Kisalföld Basin, western Hungary. – *Open-file Report 92-250, U.S. Geological Survey.* https://doi.org/10.3133/ofr92250

Ratschbacher, L., Behrmann, J. H. & Pahr, A. 1990: Penninic windows at the eastern end of the Alps and their relation to the intra-Carpathian basins. – *Tectonophysics* **172,** 91–105. https://doi.org/10.1016/0040-1951(90)90061-C

Reynolds, S. J. & Lister, G. S. 1990: Folding of Mylonitic Zones in Cordilleran Metamorphic Core Complexes – Evidence from near the Mylonitic Front. – *Geology* **18/3,** 216–219. https://doi.org/10.1130/0091-7613(1990)018<0216:Fomzic>2.3.Co;2

Schmidt, W. J., Pahr, A. & Koller, F. 1984: Die großtektonischen Zuordnung des Hannersdorfer Komplexes im Grenzbereich Österreich (Burgenland) / Ungarn. – *Mitteilungen der Österreichischen Geologischen Gesellschaft* **77,** 57–61.

Schönlaub, H. P. 2000: *Burgenland. Bundesländserie*. – Geologischen Bundesanstalt, Wien

Selverstone, J., Axen, G. J. & Luther, A. 2012: Fault localization controlled by fluid infiltration into mylonites: Formation and strength of low-angle normal faults in the midcrustal brittle-plastic transition. – *Journal of Geophysical Research–Solid Earth* **117/B6**. https://doi.org/10.1029/2012JB009171

Spear, F. S. & Pyle, J. M. 2002: Apatite, monazite, and xenotime in metamorphic rocks. – *Reviews in Mineralogy and Geochemistry* **48,** 293–335. https://doi.org/10.2138/rmg.2002.48.7

Sugisaki, R., Ido, M., Takeda, H., Isobe, Y., Hayashi, Y., Nakamura, N., Satake, H. & Mizutani, Y. 1983: Origin of hydrogen and carbon dioxide in fault gases and its relation to fault activity. – *The Journal of Geology* **91,** 239–258. https://doi.org/10.1086/628769

Tari, G. 1996a: Neoalpine tectonics of the Danube Basin (NW Pannonian Basin, Hungary). – In: Ziegler, P. & Horváth, F. (eds): Peri-Tethys Memoir 2: Structure and prospects of Alpine Basins and forelands. – *Muséum National d'histoire Naturelle* **170,** 439–454.

Tari, G. 1996b: Extreme crustal extension in the Rába River extensional corridor (Austria/Hungary). – *Mitteilungen der Gesellschaft der Geologie- und Bergbaustudenten in Österreich* **41,** 1–17.

Tari, G. 2023: *A természetes hidrogén kutatása, Tari Gábor külső tag akadémiai székfoglaló előadása*. – https://mta.hu/akademiai_szekfogalok/a-termeszetes-hidrogen-kutatasa-tari-gabor-kulso-tag-szekfoglalo-eloadasa-112995 (accessed on March 20, 2024)

Tari, G. & Bally, A. W. 1990: Metamorphic core complexes at the boundary of the Eastern Alps and the Pannonian basin. – *Geological Society of America Abstracts with Programs* **22,** 97–98.

Tari, G., Horváth, F. & Rumpler, J. 1992: Styles of extension in the Pannonian Basin. – *Tectonophysics* **208,** 203–219. https://doi.org/10.1016/0040-1951(92)90345-7

Tari, G., Dövényi, P., Dunkl, I., Horváth, F., Lenkey, L., Stefanescu, M., Szafián, P. & Tóth, T. 1999: Lithospheric structure of the Pannonian basin derived from seismic, gravity and geothermal data. – *Geological Society, London, Special Publications* **156/1,** 215–250. https://doi.org/10.1144/GSL.SP.1999.156.01.12

Tari, G. C., Gjerazi, I. & Grasemann, B. 2020: Interpretation of vintage 2D seismic reflection data along the Austrian–Hungarian border: Subsurface expression of the Rechnitz metamorphic core complex. – *Interpretation* **8/4,** SQ73–SQ91. https://doi.org/10.1190/int-2020-0029.1

Van den Kerkhof, A. M., Touret, J. L. R., Maijer, C. & Jansen, J. B. H. 1991: Retrograde methane-dominated fluid inclusions from high-temperature granulites of Rogaland, southwestern Norway. – *Geochimica et Cosmochimica Acta* **55/9,** 2533–2544. https://doi.org/10.1016/0016-7037(91)90371-b

Whitney, D. L., Teyssier, C., Rey, P. & Buck, W. R. 2013: Continental and oceanic core complexes. – *GSA Bulletin* **125/3–4,** 273–298. https://doi.org/10.1130/b30754.1

Zhang, N., Tian, Z., Leng, Y., Wang, H., Song, F. & Meng, J. (2007): Raman characteristics of hydrocarbon and hydrocarbon inclusions. – *Science in China Series D: Earth Sciences* **50,** 1171–1178. http://dx.doi.org/10.1007/s11430-007-0078-9

Manuscript received: 20/03/2024